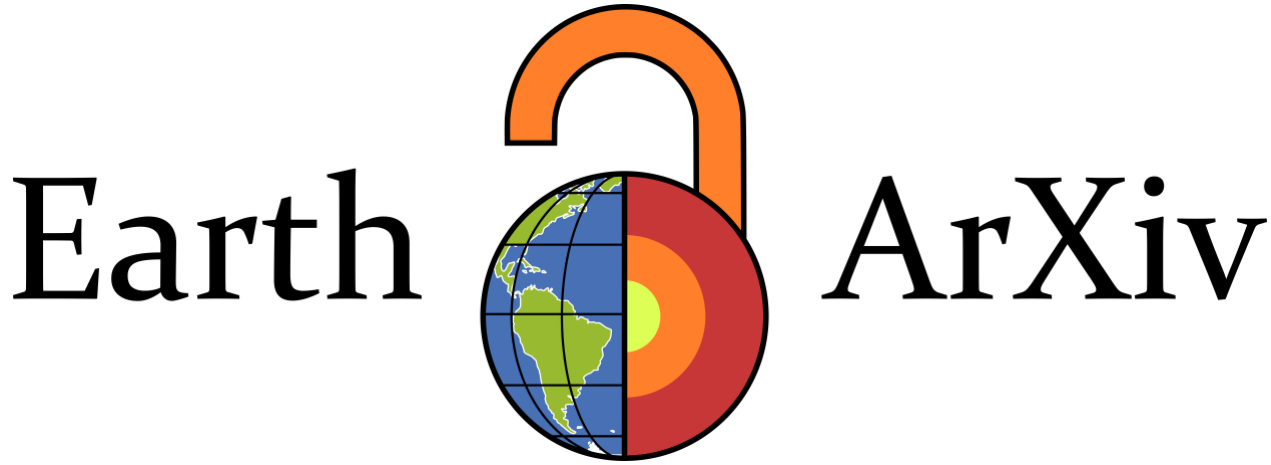

Last Interglacial shoreline successions in southeastern Australia: A framework for identifying a waning mantle plume, neotectonic movements and sea-level change

Nicolas Flament[1] and Colin V. Murray-Wallace[1]

[1]Environmental Futures, University of Wollongong, Northfields Avenue 2522 Australia

Highlights:

- MIS 5e sea level reached 4 ± 1 m above present sea level in southeastern Australia.
- There is no evidence for two sea-level peaks during MIS 5e times in southeastern Australia.
- Elevated Tasmanian MIS 5e successions relate to the waning Cosgrove mantle plume.
- Volcanism caused differential uplift of the Woakwine Range, on the Coorong coastal plain since MIS 5e times.
- Neotectonic movements are evident on Fleurieu Peninsula, southern Mount Lofty Ranges.

Abstract

Relict shoreline successions are critically important for investigations of recent tectonism, as they are commonly amenable to dating and may provide information about surface displacement and changes in sea level since their deposition. In this study, Last Interglacial (MIS 5e; 128–116 ka) shoreline successions from 47 locations across southeastern Australia are reviewed. The surface displacement of shoreline successions since their deposition is inferred from their present-day elevation and paleosea levels derived from sedimentary lithofacies and molluscan faunal assemblages. The paleosea levels suggest that MIS 5e sea level peaked at 4 ± 1 m above present sea level in southeastern Australia, about two metres lower than the commonly assumed global sea level maximum. Limited postglacial adjustment in this extreme far-field region most likely explains these observations. There is no evidence for two MIS 5e sea-level peaks in paleoshoreline successions from southeastern Australia.

The inferred uplift since MIS 5e is largest in Tasmania (up to 31 m), where it is likely caused by the waning Cosgrove mantle plume. Combining seismic tomographic models and MIS 5e shoreline data suggest that the Cosgrove mantle plume is presently centred under northeastern Tasmania, farther east than previously proposed. Volcanism above a steep gradient in lithospheric thickness caused about 10 m of eastward upward tilt of the Woakwine Range on the Coorong coastal plain since MIS 5e times. On the Fleurieu Peninsula, 6.5 m of upward displacement of the block to the southeast of the Willunga Fault is inferred. In contrast, the Gawler Craton stands out as tectonically stable, with possible limited local subsidence. The careful characterisation of shoreline successions is a powerful way to define subtle geodetic changes.

Keywords

Last Interglacial; MIS 5e; Sea level change; Paleoshoreline successions; neotectonics; mantle plumes; volcanism; stratigraphy; amino acid racemization; residual topography; dynamic topography; coastal landscape evolution

1. Introduction

Australia has traditionally been regarded as a tectonically highly stable continent (Ollier, 1978; Ollier, 1986; Twidale, 2007). Apart from its northern margin, the continent is situated within an intraplate setting, remote from plate boundaries. Other indicators of tectonic stability include the absence of recent volcanism, low seismicity, the lowest topographical relief of all continents, deeply eroded fold belts and regionally extensive erosion surfaces, as well as the antiquity of drainage systems, landscapes, relict soils, and regolith. Despite these regionally distinctive landscape characteristics, subtle evidence for neotectonism has been documented from across the continent, particularly in the coastal realm (Gardner et al., 2009; Murray-Wallace and Belperio, 1991; Quigley et al., 2010; Sandiford, 2003; Whitney and Hengesh, 2015).

In a global context, relict shoreline successions and landforms have become increasingly important for investigations of recent tectonism, as they are commonly amenable to dating and may provide critical information about geodetic changes through time, based on well-defined paleosea level indicators and marine oxygen isotope evidence for former sea levels based on ice volumes (Lisiecki and Raymo, 2005). The present-day elevation of relict shorelines indicates the cumulative eustatic and relative sea-level changes since their formation (e.g. Pedoja et al., 2014; Rovere et al., 2023). Paleoshorelines in tectonically active regions have been commonly used to infer rates of tectonic uplift (Bordoni and Valensise, 1999; Chappell, 1974; Saputra et al., 2022) and in tectonically quiescent regions can be used to examine the

93 interplay between eustatic (ice-equivalent) sea-level change and large-scale processes such as
94 glacial isostatic adjustment and mantle dynamic topography (Dutton et al., 2015). Here we
95 focus on the Last Interglacial period that corresponds with Marine Isotope Substage 5e
96 (MIS 5e; c. 128–116 ka ago), during which marine corals had lighter $\delta^{18}O$ values (e.g.
97 Shackleton et al., 2002), and eustatic sea level was higher than in the present Holocene
98 Interglacial (Kopp et al., 2009), possibly with two sea level peaks during that period (Kopp et
99 al., 2013). In this work, the Last Interglacial coastal record for a portion of the southern
100 Australian passive continental margin at the trailing edge of a fast-moving plate is reviewed.
101 A regional data set is used to infer the geographical extent of the Cosgrove mantle plume, as
102 well as other processes responsible for neotectonism along the continental margin.

103 Southeastern Australia comprises tectonically quiescent provinces such as the Gawler
104 Craton (Fig. 1), regions presenting neotectonic activity such as the Mount Lofty and Flinders
105 Ranges of the Adelaide Fold Belt (Bourman and Lindsay, 1989; Rajabi et al., 2017; Sandiford,
106 2003; Fig. 1) and former volcanic activity towards the southern termination of Earth's longest
107 continental hotspot track (the Cosgrove hotspot track; Davies et al., 2015) between ~7.9 Ma
108 and ~800 ka in the Newer Volcanic Province (Heath et al., 2020) and as recently as ~5,000
109 years ago at Mount Gambier and Mount Schank (Barbetti and Sheard, 1981; Murray-Wallace,
110 2011; Robertson et al., 1996). The elevation of Last Interglacial shoreline successions in
111 southeastern Australia has been extensively studied (e.g., Gardner et al., 2009; Goodwin et al.,
112 2023; Kiernan and Lauritzen, 2001; Murray-Wallace, 2002), making it possible to investigate
113 the relationship between tectonic or geodynamic environments and paleoshoreline elevations
114 across different geological provinces. Besides the confident identification and dating of these
115 sedimentary successions, sufficient time has elapsed since their deposition to quantify even
116 slow rates of geodetic change.

The geotectonic processes responsible for the differential elevations of Last Interglacial coastal successions in southeastern Australia, and their inferred paleosea levels are reviewed in this work. Accordingly, several attributes are explored to identify the basis for differential paleoshoreline elevations, including earthquake and fault data, the distribution of volcanism at the continental-scale, as well as continental-scale models of crustal and lithospheric thickness, and residual and dynamic topography. A representative value for ice-equivalent MIS 5e sea level is also defined for the region. This synthesis is based on our previously published research, our more recent field observations, integrated with the wider literature.

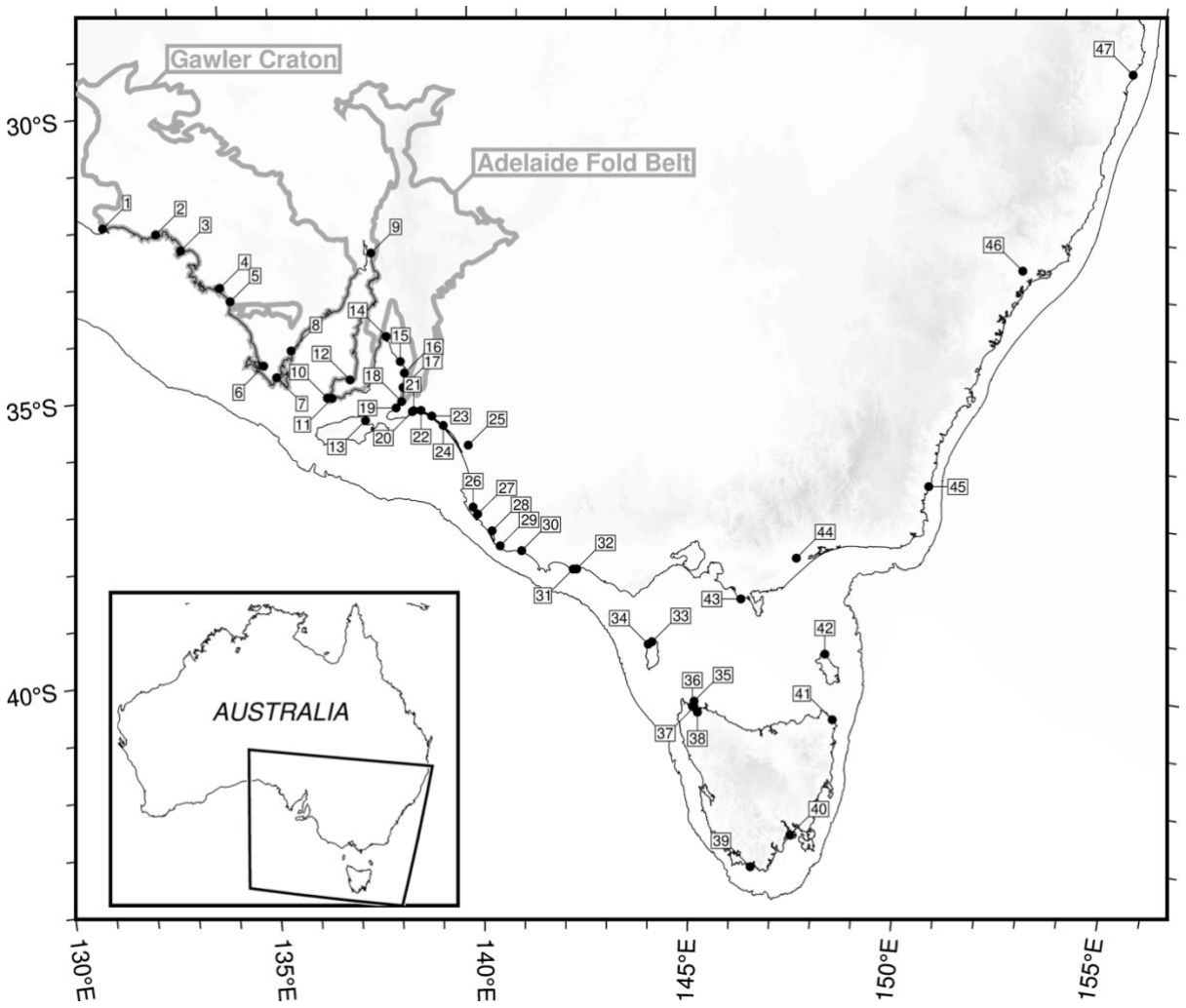

Figure 1. Locations of Last Interglacial shoreline successions in southeastern Australia reviewed in this work. Digital Elevation Model (GA, 2019) and Last Interglacial shoreline successions at 47 locations (Table 1): 1. Fowlers Bay, 2. Tourville Bay, 3. Smoky Bay, 4. Venus Bay, 5. Lake Newland, 6. Coffin Bay, 7. Port Lincoln, 8. Tumby Bay, 9. Redcliff, 10. Pondalowie Bay, 11. Marion Lake, 12. Point Turton - Hardwicke Bay, 13. Rolls Point

(Kangaroo Island), 14. Port Wakefield, 15. Port Gawler, 16. Port Adelaide, 17. Port Stanvac, 18. Sellicks Beach, 19. Normanville, 20. Chiton Rocks, 21. Victor Harbor, 22. Hindmarsh Island, 23. Mark Point, 24. Bonney Reserve, 25. Salt Creek, 26. Lake Hawdon South, 27. McCourt Cutting (Woakwine Range), 28. Lake Bonney, 29. Nene Valley, 30. Nelson, 31. Goose Lagoon, 32. Warrnambool, 33. Egg Lagoon (King Island), 34. Yellow Rock River (King Island), 35. Robbins Island, 36. Montagu, 37. Mowbray Swamp, 38. Broadmeadows, 39. New River Lagoon Sea Caves, 40. Mary Ann Bay, 41. Stumpys Bay, 42. North East River (Flinders Island), 43. Liptrap, 44. Sale, 45 Gillard's Beach, 46. Largs, 47. Evans Head. The Gawler Craton and Adelaide Fold Belt regions at the 1:5 million scale (Blake, 1998) are shown as grey polygons. The inset shows the map area in the context of Australian coastlines.

Table 1. Locations, age, upper bounding surface elevation, inferred paleosea level, inferred surface displacement and paleosea level indicator for Last Interglacial shoreline successions in southeastern Australia. Paleosea levels are inferred from sedimentary facies. Last interglacial shoreline elevations and inferred paleosea levels APSL (m) are based on molluscan fossil assemblages. 'APSL': above present sea level; 'SA': South Australia; 'VIC': Victoria; 'TAS': Tasmania; NSW: New South Wales.

Location number and name	Latitude and Longitude	Age	Elevation of upper bounding surface of sedimentary unit (m APSL)	Inferred MIS 5e sea level (m APSL)	Inferred surface displacement (m)	Paleosea level indicator	Reference
1. Fowlers Bay, SA	S31°57'06.9" E132°20'40.6"	113±8 ka U-Series	0.16	2.1±0.5	-1.74	Relict back-barrier lagoonal sandflat facies with *Katelysia rhytiphora* and *Anadara trapezia*	Murray-Wallace et al. (2016)
2. Tourville Bay, SA	S32°08'14.5" E133°25'52.0"	MIS 5e AAR	2.55	4±0.5	2.55	Relict intertidal sandflat facies with *Katelysia rhytiphora* and *Anadara trapezia.*	Belperio et al. (1995); Murray-Wallace et al. (2016)
3. Smoky Bay, SA	S32°27'31.4" E133°55'24.4"	MIS 5e AAR	1.9	3.4±0.5	1.3	Intertidal to shallow subtidal mud flat facies with *Katelysia* sp., *Batillaria* sp.	Murray-Wallace et al. (2016)
4. Venus Bay, SA	S33°10'09.8" E134°40'55.7"	Correlation by litho- and biostratigraphy	2.0	3.5±0.5	1.5	Intertidal shelly facies beneath calcrete	Belperio et al. (1995)
5. Lake Newland, SA	S33°25'13.4" E134°52'55.8"	112±10 ka U-Series *Anadara trapezia* MIS 5e AAR	1.9	3.5±0.5	1.4	Intertidal lagoon facies with *Anadara trapezia* and *Katelysia* sp. beneath calcrete	Murray-Wallace et al. (2016)

6. Coffin Bay, SA	S34°35'55.80" E135°30'9.08"	Correlation by litho- and biostratigraphy	2.0	3.5±0.5	1.5	Intertidal shelly sandflat facies beneath calcrete	Belperio et al. (1995)
7. Port Lincoln, SA	S34°49'5.70" E135°45'51.44'	Correlation by litho- and biostratigraphy	1.0	2±0.5	-1	Intertidal shelly sands beneath calcrete	Belperio et al. (1995)
8. Tumby Bay, SA	S34°21'39.12" E136°6'24.36"	Correlation by litho- and biostratigraphy	0.5	2±0.5	-1.5	Intertidal shelly sands beneath calcrete	Belperio et al. (1995)
9. Redcliff, northern Spencer Gulf, SA	S32°41'39.38" E137°54'2.78"	Correlation by litho- and biostratigraphy	2.0	4±1	2	Intertidal to shallow subtidal facies with *Anadara trapezia* and *Marginopora vertebralis* in Redcliff Core Red 51.	Belperio et al. (1995)
10. Pondalowie Bay, SA	S35°13'58.0" E136°49'53.0"	Correlation by litho- and biostratigraphy	1.5	4±1	1.5	Shallow subtidal facies with *Eucrassatella* sp., *Venerupis* sp., and *Thalotia* sp., beneath calcrete	This study
11. Marion Lake, SA	S35°14'28.10" E136°56'6.70"	Correlation by litho- and biostratigraphy	2.5	4±1	2.5	Intertidal shelly facies beneath calcrete	Belperio et al. (1995)
12. Point Turton, Hardwicke Bay, SA	S34°55'47.8" E137°20'26.5"	127.3±2.1 to 115±5.4 ka U-Series & AAR	2.9	4.8±1	3.7	Upward deepening transition from intertidal to shallow subtidal facies with *Batillaria* sp., *Katelysia* sp., and *Amesodesma angusta*.	Pan et al. (2018)
13. Rolls Point, Kangaroo Island, SA	S35°39'37.59" E137°38'3.35"	122±1 ka U-Series	3.4	3.1±0.04	2.5	Shingle beach facies	Nicholas et al. (2019)
14. Port Wakefield, SA	S34°11'10.9" E138°09'24.3"	MIS 5e AAR	3–4.6	3±1	3.6	Top of laminar calcrete on gravel beach ridges with *Anadara trapezia.*	Murray-Wallace and Belperio (1991); Belperio et al. (1995)
15. Port Gawler, SA	S34°38'21.93" E138°26'11.94"	Correlation by litho- and biostratigraphy	2.0	3±0.5	1	Shelly intertidal facies beneath calcrete	Belperio et al. (1995)

16. Port Adelaide, SA	S34°50'53.27" E138°30'55.45"	Correlation by litho- and biostratigraphy	-1.2–2.1	2±0.5	0.1	Intertidal shelly sands beneath calcrete	Ludbrook (1976)
17. Port Stanvac, SA	S35°6'8.18" E138°28'36.74"	Correlation by litho- and biostratigraphy	3.8	4±1	3.8	Intertidal to shallow subtidal shelly facies beneath calcrete	Belperio et al. (1995)
18. Sellicks Beach, SA	S35°21'09.8" E138°26'07.5"	MIS 5e AAR	5.5	4±1	5.5	Bevelled platform surface with overlying fossiliferous shingle-gravel beach facies	Murray-Wallace and Bourman (2002)
19. Normanville, SA	S35°27'43.54" E138°18'34.27"	MIS 5e AAR	12	4±1	12	Shelly embayment fill facies	Bourman et al. (1999)
20. Chiton Rocks, SA	S35°32'10.0" E138°39'39.6"	MIS 5e AAR	8.0	3±1	7	Relict estuarine facies with *Anadara* sp.	Murray-Wallace et al. (2010)
21. Victor Harbor, SA	S35°31.33'.43" E138°41'15.40"	MIS 5e AAR	6.0	3±1	5	Relict estuarine facies with *Anadara* sp.	Murray-Wallace et al. (2010)
22. Hindmarsh Island, SA	S35°31'12.31" E138°50'56.49"	MIS 5e AAR	1.0	3±0.5	0	Estuarine intertidal facies with *Katelysia scalarina* beneath calcrete	Murray-Wallace et al. (2010)
23. Mark Point, SA	S35°37'37.01" E139°4'45.27"	MIS 5e AAR	1.9	3±0.5	0.9	Planar and trough cross bedded lower foreshore facies with *in situ Donax deltoides*	Murray-Wallace et al. (2010)
24. Bonney Reserve, SA	S35°47'58.72" E139°19'19.16"	Correlation by litho- and biostratigraphy	3.8	3±0.5	2.8	Planar and trough cross bedded lower foreshore facies with *in situ Donax deltoides*	(Bourman et al., 2000)
25. Salt Creek, SA	S36°09'40.1" E139°51'30.6"	MIS 5e AAR	4.6	3±0.5	3.6	Relict beach facies of Woakwine Range with transported *Anapella* sp.	Murray-Wallace and Cann (2007); Murray-Wallace (2018)
26. Lake Hawdon South, SA	S37°15'44.4" E139°56'10.7"	MIS 5e AAR	5–7.0	3±0.5	6	Back-barrier intertidal to subtidal lagoon facies of Woakwine Range	Murray-Wallace (2018)
27. McCourt Cutting, Woakwine Range, SA	S37°15'43.8" E139°56'12.6"	117±8 ka TL MIS 5e AAR	6.4 to 11.6	3±0.5	11.6	Transgression from 6.4 to 11.6 m APSL. Upper surface of back-barrier lagoon facies with	Murray-Wallace et al. (1999)

						articulated *Katelysia* sp. in growth position.	
28. Lake Bonney, SA	37°41'24.45" E140°20'58.22"	Correlation by litho- and biostratigraphy	13	3±0.5	12	Intertidal shelly facies beneath calcrete of Glanville Formation	Murray-Wallace et al. (1996a)
29. Nene Valley, SA	S37°59'55.04" E140°33'42.86"	Correlation by litho- and biostratigraphy	18	≥3±1	17	Top of shelly facies of Glanville Formation	Murray-Wallace et al. (1996a)
30. Nelson, VIC	S38°2'58.92" E141°0'25.42"	Correlation by litho- and biostratigraphy	4	3±0.5	3	Lithified Intertidal shelly sands	Murray-Wallace et al. (1996a)
31. Goose Lagoon, VIC	S38°22'50.30" E142°9'52.19"	101±2.6 ka U/Th 110±17 ka Pa/Th MIS 5e by AAR	3.7–4.2	3±1	3.2	Intertidal to shallow subtidal molluscan shell bed with *Katelysia rhytiphora* and *Batillaria (Zeacumantus) diemenensis*	Sherwood et al. (1994)
32. Warrnambool, VIC	S38°22'42" E142°14'34"	Correlation by Litho-and Biostratigraphy	7.5	3±1	6.5	Marine molluscs including *Ninella torquata* in Port Fairy Calcarenite immediately above a shore platform cut on Port Campbell Limestone	Gill (1988)
33. Egg Lagoon, King Island, TAS	S39°39'22.87" E143°58'34.88"	MIS 5e AAR & ESR	6	4±1	6	Intertidal to shallow subtidal shelly sands with *Katelysia rhytiphora* and *K. scalarina*	Murray-Wallace and Goede (1995)
34. Yellow Rock River, King Island, TAS	S39°41'58.46" E143°53'32.07"	MIS 5e AAR and ESR	3.5	4.5±0.5	4	Intertidal to shallow subtidal bioclastic shelly sands with *Katelysia rhytiphora* and *K. scalarina*	Murray-Wallace and Goede (1995)
35. Remarkable Banks beach ridge plain, Robbins Island, TAS	S40°41'7.87" E144°59'10.28"	OSL	11	5.75±0.5	12.75	Intertidal beach facies seaward of each relict beach ridge	Goodwin et al. (2023)
36. Montagu, TAS	S40°46'39.45" E144°57'9.87"	MIS 5e AAR and ESR	12	4±1	12	Mella Sand, Shallow subtidal embayment fill	Murray-Wallace and Goede (1995)
37. Mowbray Swamp, TAS	S40°47'28.74" E144°59"32.61'	MIS 5e AAR and ESR	12	4±1	12	Mella Sand, Shallow subtidal embayment fill	Murray-Wallace and Goede (1995)

38. Broadmeadows, TAS	S40°52.7'7.49" E145°4'30.56"	MIS 5e AAR and ESR	13	4±1	13	Mella Sand, Shallow subtidal embayment fill	Murray-Wallace and Goede (1995)
39. New River Lagoon Sea Caves, TAS	S43°29'07" E146°35'13"	121.76 +6.07 -5.80 ka U-Series	<10	>3	7	Coastal sourced gravels and shingle beneath speleothem and stalagmite in Bahaus Cave	Kiernan and Lauritzen (2001)
40. Mary Ann Bay, TAS	S42°58'28.18" E147°23'47.75"	MIS 5e AAR and ESR	24.5	≥2	22.5	Lower shoreface sands with shell rich planar cross beds	Murray-Wallace and Goede (1995)
41. Stumpys Bay, TAS	S40°53'39.08" E148°13'26.59"	Inferred MIS 5e	32	3±1	31	Relict quartz beach ridges of the Stumpys Bay Sand	Bowden and Colhoun (1984)
42. North East River, Flinders Island, TAS	S39°44'43.36" E147°57'22.53"	MIS 5e AAR and ESR	4.5	4±1	4.5	Intertidal to shallow subtidal bioclastic shelly sands with *Katelysia rhytiphora* and *K. scalarina* and *Batillaria (Zeacumantus) diemenensis*	Murray-Wallace and Goede (1995)
43. Liptrap, VIC	S38°50'48.69" E145°58'30.89"	OSL	7.25	(3.45±1)	6.7	(Average of sea level at all other locations)	Gardner et al. (2009)
44. Lake Wellington Main Drain, West of Lake Melanydra, Sale, VIC	S38°04'35" E147°10'45"	125 ka on *Neotrogonia* sp. U-Series	7.6	3±1	6.6	Estuarine shell bed with *Ostrea sinuata.*	Schornick (1973); Jenkin (1988)
45. Middle Lagoon at Gillard's Beach, NSW	S36°39'02" E150°00'24"	114±15 ka 126±13 ka TL	4.8	3	3.8	Beach facies with cobbles and stringers of pebbles	Young et al. (1993)
46. Largs, Hunter Valley, NSW	S32°42'14.62" E151°36'23.44'	MIS 5e AAR	4–5	5.5±0.5	6.5	Intertidal estuarine shell bed with *Anadara trapezia*	Thom and Murray-Wallace (1988); Murray-Wallace et al. (1996b)
47. Evans Head, NSW	S28°04' E153°27'	112±9 to 127±18 ka U-Series	c. 0	5±1	1	Corals *Montipora* sp. *Platygyra lamellina* *Acropor a* sp. *Pocillopora damicornis*	Marshall and Thom (1976)

147

2. Data

2.1. Nature and Age of Last Interglacial coastal successions in southeastern Australia (locations 1–32)

2.1.1. General context

Last Interglacial coastal sedimentary successions and landforms are particularly well-preserved along the cool water, temperate carbonate realm of southern Australia (Belperio et al., 1995; Murray-Wallace and Belperio, 1991). In this region, extensive pedogenic calcrete development has provided a protective carapace to the underlying fossiliferous carbonate successions, reducing their susceptibility to erosion. Last Interglacial coastal successions occur landward of Holocene coastal complexes and reflect a higher relative sea level than in the present, Holocene Interglacial. The intertidal and shallow subtidal, estuarine-lagoonal back-barrier facies (open ocean coastline), and peritidal sand and mudflat facies (protected gulfs) have been mapped as the Glanville Formation (Belperio et al., 1995). Correlative interdigitated bioclastic carbonate dune facies (aeolianites) have been mapped as the Upper Member of the Bridgewater Formation (Sprigg and Boutakoff, 1953). An overview of the literature on the Pleistocene Bridgewater Formation is provided elsewhere (Murray-Wallace, 2018).

Woods (1862; later publishing as Tenison-Woods), Tate (1879a), Tate (1879b), Tate (1882), Howchin (1888) and Greenway and Phillipps (1902) identified distinctive shelly limestones cropping out along extensive sectors of the southern Australian coastline that were potentially of equivalent age and representing an ‘upheaval of the land’ (Tate, 1879a, p. lxviii). Many workers have since documented the field relationships of numerous occurrences of lithologically and palaeontologically similar sedimentary successions, now assigned to the Glanville Formation (Belperio et al., 1995; Blakemore et al., 2015; Bourman et al., 2016; Ludbrook, 1984; Murray-Wallace and Belperio, 1991; Murray-Wallace et al., 2016; Nicholas et al., 2019; Pan et al., 2021; Pan et al., 2018).

2.1.2. The Glanville Formation

The Glanville Formation *sensu* Firman (1966) was first described in the Adelaide region of Gulf St Vincent, in an excavation for Fletcher's Graving Dock at Glanville, in the Inner Harbor at Port Adelaide (Howchin, 1888; Ludbrook, 1976). Within the depth interval of 10.05–11.27 m below the ground surface, the section revealed calcareous sand with a diverse molluscan fauna beneath a prominent calcrete, representing the top of the formation and a subaerial exposure surface. Most of the fossil marine mollusc species have modern equivalents. The presence of some species no longer living in the coastal waters of South Australia, such as the Sydney Blood cockle *Anadara trapezia* (originally termed *Arca trapezia*; Howchin 1888; Tate, 1882), Shark Bay pearl oyster *Pinctada carchariarum*, the Rosemouth star shell *Astralium rhodostomum*, conical-fusiform gastropod *Euplica bidentata*, and the benthic foraminifers *Marginopora vertebralis* (originally termed *Orbitolites complanata*; Howchin 1888) and *Quinqueloculina polygona*, led several researchers to describe the faunal assemblages as 'Sub-Recent' or 'Sub-fossil' (Howchin, 1888; Ludbrook, 1984; Tate, 1879a). The shallow depth of the formation below present sea level at the Glanville Graving Dock indicates that the Glanville Formation at this locality represents a transgressive succession before the culmination of post-Stage 6 sea-level rise. Post-depositional subsidence of the Adelaide Plains since the Last Interglacial may also have contributed to the lower topographical level of the succession (Belperio, 1993).

In the terminology of Sequence Stratigraphy (Coe, 2003), the Glanville Formation represents a parasequence, reflecting the interplay of sediment supply and the production of sedimentary carbonate in relation to accommodation space associated with relative sea-level changes during MIS 5e. In Spencer Gulf and Gulf St Vincent, the base of the Glanville Formation is commonly represented by an unconformable contact (a thin transgressive facies or flooding surface) with underlying Middle Pleistocene alluvial successions such as the

198 Hindmarsh Clay, representing distal alluvial fans of the Mount Lofty and Flinders Ranges
199 (Firman, 1966; Hails et al., 1984). The calcreted top of the Glanville Formation, representing
200 a subaerial exposure surface, is characteristically overlain by contemporaneous Upper
201 Pleistocene or unconformably, by younger successions of the alluvial Pooraka Formation, or
202 coastal facies of the Holocene St Kilda Formation (Bourman et al., 2010; Cann and Gostin,
203 1985). Marine vibracores from Gulf St Vincent show that the calcrete developed on the upper-
204 most portion of the Glanville Formation dips gently towards the central portion of the gulf,
205 revealing an antecedent topography defined by this calcareous hardground surface, and
206 influencing the geometry of younger Late Pleistocene and Holocene successions (Murray-
207 Wallace et al., 2021).
208 Before the application of geochronological methods, the Glanville Formation was
209 presumed to be of Last Interglacial age based on distinctive warmer-water fossil assemblages
210 and lithological properties not evident in younger successions (Belperio et al., 1995). The
211 Glanville Formation can be traced laterally for over 1,500 km along the coastline of South
212 Australia including Hindmarsh (location 22) and Kangaroo islands (location 13). The western-
213 most location of the formation is at the Head of the Great Australian Bight at Yalata Swamp,
214 where richly fossiliferous shelly limestones containing *Anadara trapezia*, capped by a 23 cm
215 thick calcrete, crop out up to 2 m above present sea level (APSL) (Tate, 1879b).
216
217 *2.1.3. Gawler Craton to Yorke Peninsula (locations 1–15)*
218 The Glanville Formation occurs from near the modern coastline up to several
219 kilometres inland on depositional coasts, or within coastal cliffs on eroding coasts (Belperio et
220 al., 1995; Bourman et al., 2016; Murray-Wallace, 2018; Pan et al., 2018). On western Eyre
221 Peninsula, the Glanville Formation occurs as back-barrier estuarine-lagoonal successions and
222 at Fowlers Bay (location 1) was also deposited in the lee of Middle Pleistocene barrier

complexes (Murray-Wallace et al., 2016; Figs 2–3). On the northern Adelaide plains, the Glanville Formation indicates subsidence of this region (Belperio et al., 1995). At Sandy Point near the apex of Gulf St Vincent, the top of the Glanville Formation occurs between c. 1.5–2 m APSL. In the Port Wakefield Proof Range area near Sandy Point (location 14), some 10 km south of Port Wakefield, former intertidal flats of the Last Interglacial Glanville Formation, up to 600 m wide in cross-section, now represent supratidal environments of the current, Holocene interglacial (Belperio, 1985; Fig. 4). The relict, calcrete capped and cemented clay-rich to micrite biocalcarenite sediments are partially karstified. The intertidal flat sediments of the Glanville Formation and the alluvial successions of the Middle Pleistocene Hindmarsh Clay represent an antecedent topography that has severely restricted the space available for the deposition of Holocene coastal sediments within the region.

Figure 2. Detached block (Sample EP#2 of Murray-Wallace et al., 2016) of Last Interglacial Glanville Formation sediment (coquina) at Fowlers Bay, western Eyre Peninsula, southern Australia (location1). Sample EP#2 was collected 7 km inland from the modern coastline, from back-barrier estuarine-lagoonal facies. The back-barrier sediments include a shell assemblage dominated by articulated specimens of the cockle *Katelysia* sp. The general character of the sediment is representative of many back-barrier facies of the Glanville Formation in South Australia.

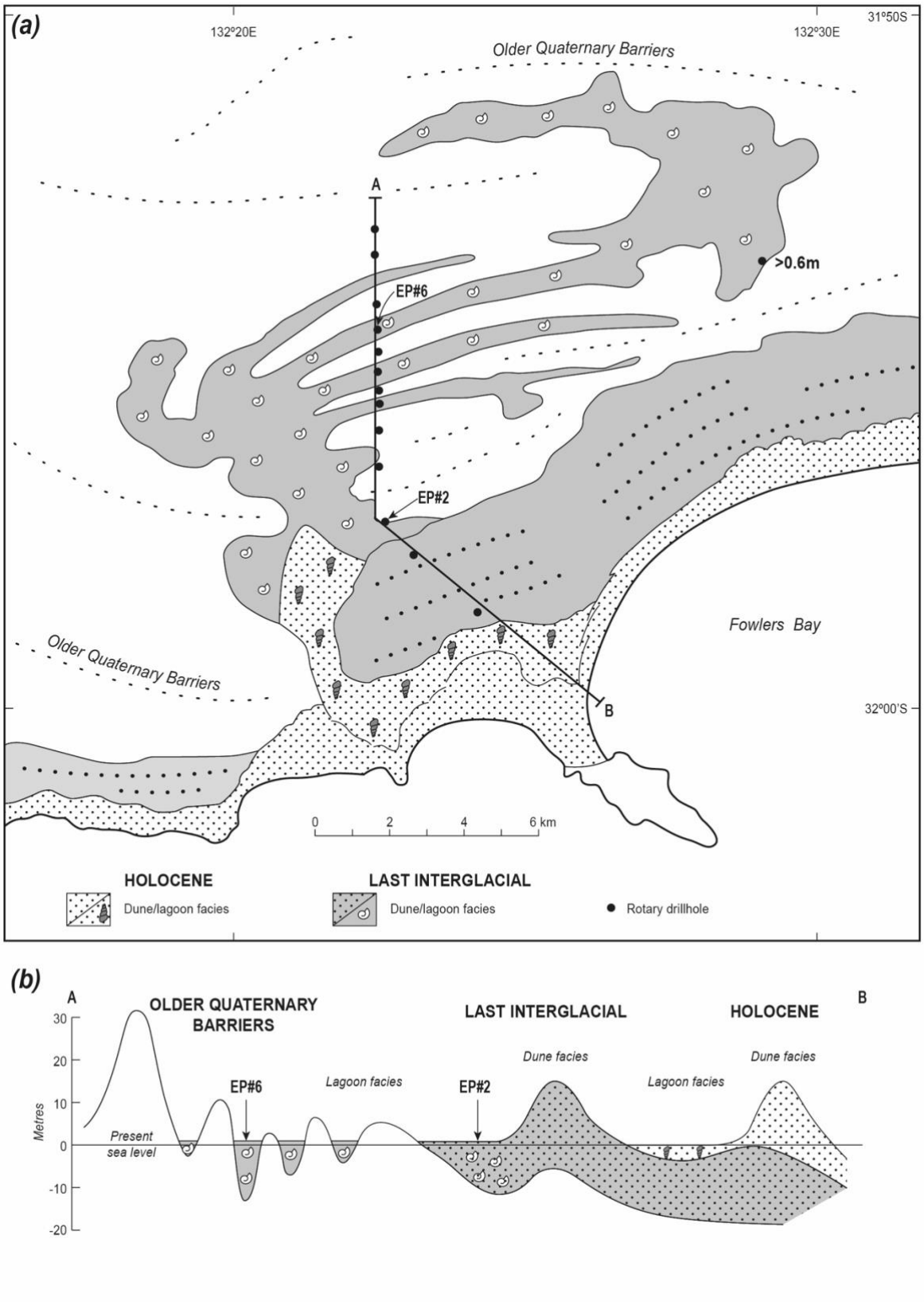

Figure 3. Map (a) and stratigraphical cross-section (b) of Fowlers Bay, western Eyre Peninsula, southern Australia (location 1). Sample EP#2 (Figure 2) is located on the landward side of the Last Interglacial barrier. The higher sea level of the Last Interglacial (MIS 5e) resulted in a marine incursion in the lee of four Middle Pleistocene aeolianite barriers (source: Murray-Wallace et al., 2016).

Figure 4. View looking south across relict intertidal flats of the Last Interglacial (MIS 5e) Glanville Formation at Sandy Point (location 14), near the apex of Gulf St Vincent, southern Australia. The modern surface at 1.5 m to 2 m APSL represents the landward limit of Holocene supratidal flats, which have formed on the calcreted surface of the Last Interglacial Glanville Formation. Minimal space has been available for Holocene coastal sedimentation.

2.1.4. Fleurieu Peninsula (locations 16–21) and Coorong Coastal Plain (locations 22–30)

Uplift of the Glanville Formation is evident at several sites on Fleurieu Peninsula. At Sellicks Beach (location 18), an emergent shingle-gravel beach deposit on a marine eroded bench, occurs at a 5.5 m APSL (Murray-Wallace and Bourman, 2002). At Normanville (location 19), 23 km SW of Sellicks Beach, a shelly sand, embayment fill succession occurs at 12 m APSL (Bourman et al., 1999). Emergent coastal successions of MIS 5e age also occur on the eastern side of Fleurieu Peninsula, at Chiton Rocks and Victor Harbor (locations 20–21) occurring at 8 m and 6 m APSL m, respectively. The Glanville Formation with a well-developed calcrete surface above a shell coquina also occurs on Dudley Peninsula, Kangaroo Island (Fig. 5f).

Last Interglacial shoreline successions and coastal landforms are particularly well-represented in southern South Australia, extending from the River Murray mouth region adjacent to Fleurieu Peninsula (De Mooy, 1959; Ryan, 2015; Sprigg, 1959), across Hindmarsh Island (location 22; Murray-Wallace et al., 2010) and south-eastwards towards Mount Gambier and Mount Schank (Hossfeld, 1950; Murray-Wallace et al., 1996a; Murray-Wallace et al., 2016; Fig. 1). Along this coastal sector, there is a progressive rise of the surface elevation of the Last Interglacial Glanville Formation from 0.17–2.94 m at Goolwa (Ryan, 2015), 1 m APSL on Hindmarsh Island (location 22), 1.9 m APSL at Mark Point (location 23; Fig. 5c), 15 km SE of Hindmarsh Island, 3.8 m at Bonney Reserve (location 24), 4.6 m at Salt Creek (location 25), 5–7 m at Lake Hawdon South (location 26), 6.4–11.6 m at McCourt Cutting (location 27), 13 m at Lake Bonney (location 28), rising to 18 m APSL at Nene Valley (location 29; Table 1).

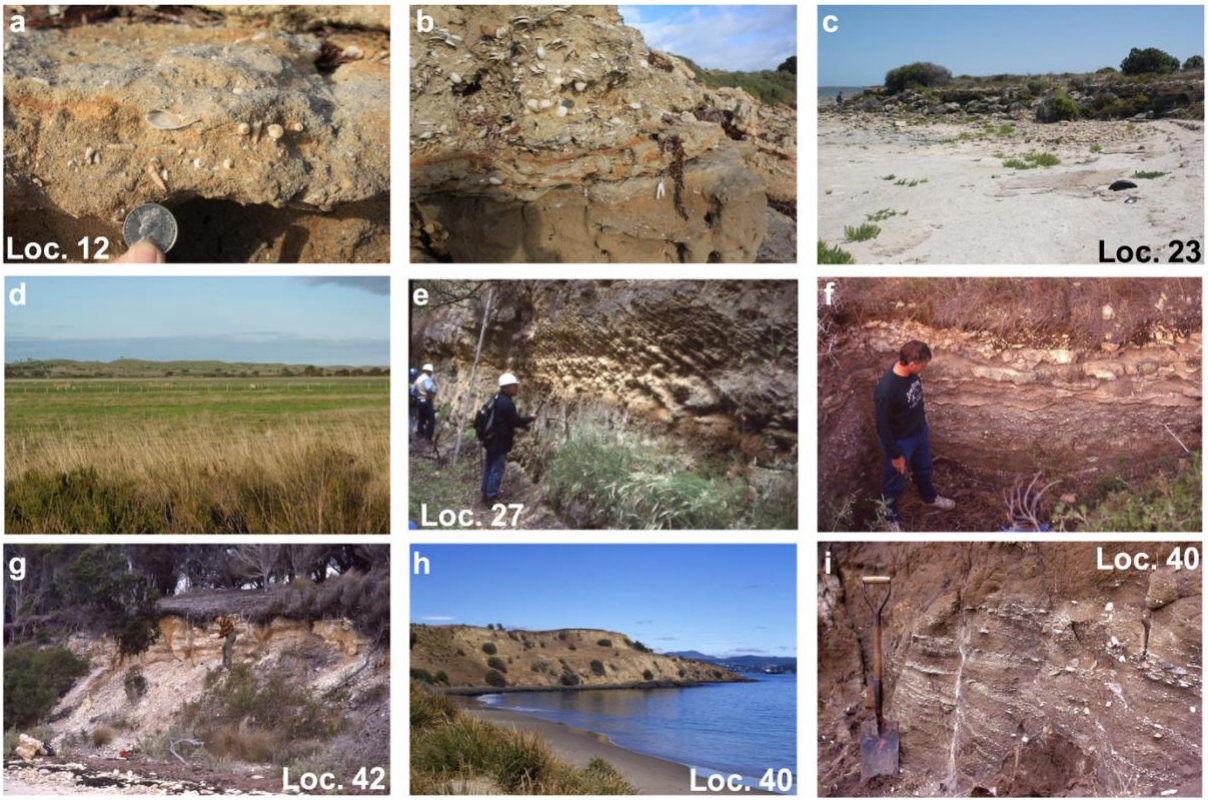

Figure 5. Last Interglacial (MIS 5e; 128–116 ka) coastal sedimentary successions and landforms in southeastern Australia. **a**, Indurated intertidal sandflat facies with the upper-

bounding surface evident, Point Turton, southern Yorke Peninsula (location 12). The turreted gastropod *Batillaria (Zeacumantus) diemenensis* in life position, formerly grazing immediately below the sediment-water interface. The former sandflat surface is 2.5 m APSL. **b**, Shallow subtidal shelly facies overlying intertidal sandflat facies approximately 70 m west of photo site 2a at Point Turton. The condensed shell bed represents a mixed concentration of *in situ* articulated and disarticulated bivalve molluscs dominated by *Katelysia scalarina* which frequents the shallow subtidal to lower intertidal zone of sandflats. The succession signifies a relative rise in sea level. The upper bounding surface of the shelly unit is 2.4 m APSL suggesting that sea level reached up to 4.8 ± 1 m APSL at the time of sedimentation. **c**, Strongly indurated, seaward dipping lower- to upper foreshore facies up to 2 m APSL at Mark Point, northern Coorong Lagoon (location 23). The laminar calcrete capped unit crops out on the landward side of the Holocene/modern Coorong Lagoon 18 km SE of the River Murray Mouth. **d**, View looking north towards the landward side of the Woakwine Range, a coastal barrier complex with relict dune surfaces reaching up to 50 m APSL. **e**, Planar cross-bedded (foreset beds) of transgressive aeolian dunes overriding back-barrier estuarine-lagoonal facies in the lee side of the Woakwine Range in the McCourt Cutting near Beachport (location 27). **f**, Small exposure of the Last Interglacial Glanville Formation 2 km east of Pelican Lagoon, Dudley Peninsula, Kangaroo Island, showing an *in situ* shelly assemblage overlain by laminar, blocky and rubbly calcrete. **g**, Shell beds dominated by *Katelysia rhytiphora* overlying oyster mounds at North East River, Flinders Island, Bass Strait, Tasmania (location 42). **h**, Emergent shelly sands up to 24.5 m APSL at Mary Ann Bay, southern Tasmania (location 40). The succession is capped by aeolian sands and overlies a bench on Jurassic dolerite. **i**, Detail of the low angle planar cross-bedded sands at Mary Ann Bay (location 40), with entire disarticulated bivalve molluscs of *Pecten meridionalis* and *Fulvia tenuicostata*.

2.1.5. The Woakwine Range (locations 22–29)

The principal Last Interglacial coastal landform in this region is the Woakwine Range, a partially lithified coastal barrier which extends uninterrupted along the landward side of the Coorong Lagoon (Fig. 5d-e). The dune range is a prominent structure (30–35 m high and 1–2 km wide) extending southeasterly for over 370 km from the River Murray mouth area to Nelson in western Victoria (locations 22 to 30; Murray-Wallace et al., 1996a). To the south of Mount Gambier, the barrier was termed the MacDonnell Range by Sprigg (1952) and has been dated at 124±10 ka by OSL on quartz sand (Blakemore et al., 2014). The only interruption in the continuity of the Woakwine Range is between Cape Jaffa and Kingston SE, where the dune range bifurcates to form an easterly trending spit or 'hook' (Benson's Hook; Fig. 6). The spit formed within a partially protected marine corridor between the Woakwine Range and Reedy Creek, an older barrier of MIS 7e age, due to longshore drift in the lower wave energy, lee-side

of the Woakwine Range at southern Lacepede Bay. During the Last Interglacial, a 20–25 km wide marine corridor existed between the actively forming Woakwine Range and the older, more landward and consolidated Reedy Creek Range (MIS 7e; Fig. 6). At this time, low energy estuarine-lagoonal successions containing *Anadara trapezia* were deposited between these dune ranges, representing the *Anadara* High Sea Level of Crocker and Cotton (1946) and (Sprigg, 1952). The basis for the break in the lateral continuity of the Woakwine Range at southern-most Lacepede Bay remains unresolved, however, it is noted that it coincides with the northern limit of the Paleogene–Neogene Gambier Embayment and may relate to subtle differences in the bathymetry of southern Lacepede Bay.

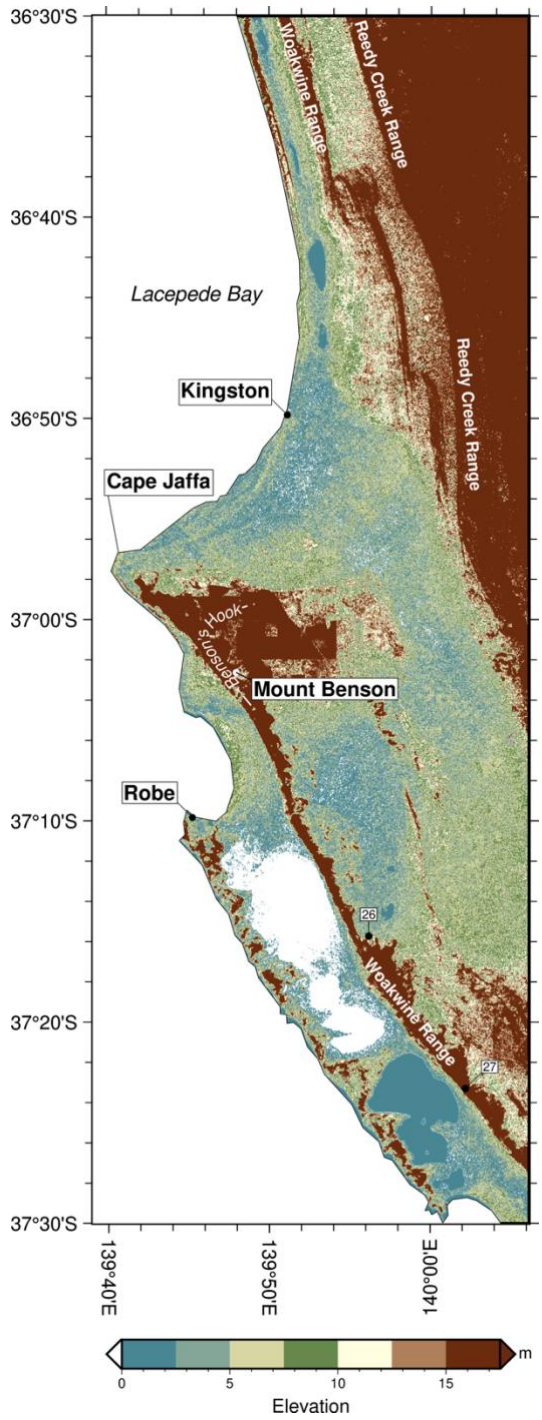

Figure 6. Digital Elevation Model (JPL, 2013) of the Coorong Coastal Plain around Kingston and Robe. The map illustrates a portion of the Last Interglacial coastal barrier, Woakwine Range. The map reveals that the Woakwine Range bifurcates at southern Lacepede Bay with the development of Benson's Hook to the east of Cape Jaffa. Back-barrier estuarine-lagoonal sediments of MIS 5e age, formed between the Woakwine Range, an aeolianite coastal barrier also of MIS 5e age and Reedy Creek, a barrier of MIS 7 age. The former coastal water way was 20–25 km wide.

340 *2.1.6. Age of the Glanville and Bridgewater Formations in South Australia*

341 The Last Interglacial age of the coastal successions reported in this study, and their
342 correlation with MIS 5e is based on uranium-series dating, thermoluminescence (TL), optically
343 stimulated luminescence (OSL), amino acid racemization (AAR), and electron spin resonance
344 (ESR). The Last Interglacial age of the Glanville Formation has been established from several
345 sites based on uranium-series dating, supplemented by regional correlation using AAR. Daniel
346 (2002) reported a uranium-series age of 124 ± 9 ka on a specimen of the coral *Goniopora* sp.,
347 from the Glanville Formation at Flagstaff Landing, Streaky Bay, western Eyre Peninsula.
348 Specimens of the robust cockle, *Anadara trapezia* from Tourville Bay, western Eyre Peninsula
349 (location 2), were dated at 120 ± 10 ka based on multi-collector, inductively coupled plasma
350 mass spectrometry (MC-ICP-MS; Eggins et al., 2005). At Point Turton, southern Yorke
351 Peninsula (location 12), uranium-series ages of 128.3 ± 2.5 ka, 127.3 ± 2.1 ka, and 121.4 ±
352 2.4 ka have been reported for corals within consolidated bioclastic sands of the Glanville
353 Formation (Pan et al., 2018; Fig. 5a). A uranium-series age of 125 ± 10 ka was obtained on
354 aragonitic fossil molluscs from back-barrier, estuarine-lagoonal sediments of the Woakwine
355 Range near Robe in southern South Australia (Schwebel, 1984).

356 Luminescence analyses on quartz sands from aeolianite of the Bridgewater Formation
357 have contributed to defining the geographical extent of the Last Interglacial shoreline in
358 southern Australia. Although the analytical precision is lower than more recently derived
359 uranium-series ages, the TL and OSL ages consistently fall within the age range of 132 ± 9 to
360 117 ± 8 ka (see overview in Murray-Wallace, 2018).

361

362 *2.1.7. Nature and basis for age of MIS 5e successions in Victoria*

363 Correlative stratigraphical successions to the Glanville Formation (MIS 5e) of South
364 Australia have been described from Victoria (Gill, 1988; Jenkin, 1988; Sherwood et al., 1994),

New South Wales (Murray-Wallace et al., 1996b; Thom and Murray-Wallace, 1988; Young et al., 1993), and Tasmania and the Bass Strait Islands (Bowden and Colhoun, 1984; Goodwin et al., 2023; Murray-Wallace and Goede, 1995; Table 1). Sedimentary successions along the eastern coastline of Victoria and New South Wales are dominantly of terrigenous-clastic origin with few calcium carbonate bioclasts.

Estuarine-lagoonal shelly successions of MIS 5e age indicating a relative sea level of up to 4.2 m APSL, have been described at Goose Lagoon, 13 km west of Warrnambool (location 31), dated at 101±2.6 ka (U/Th) and 110±17 ka (Th/Pa) and correlated with other MIS 5e shelly successions by AAR (Sherwood et al., 1994). At Warrnambool (location 32), a relative sea level of 7.5 m APSL is indicated by shelly successions within the Port Fairy Calcarenite resting on a shore platform (Gill, 1988).

Farther east, Quaternary marine terraces indicating coastal emergence have been described from Cape Liptrap, 47 km NW of Wilson Promontory in Victoria (location 43; Gardner et al., 2009). The marine abrasion platform surfaces range in elevation from 1.2 m APSL at Morgan's Beach, west of Cape Liptrap, to 7.25 m APSL at Walkerville South in Waratah Bay. The NE trending Waratah Fault has differentially elevated the latter shoreline through a scissor movement. This is illustrated by a decrease in shoreline angle, a marine eroded junction between the cliff face and landward limit of the shore platform, in a NE direction from 7.25 m to 3.2 m APSL over 2 km, parallel with the Waratah Fault. Quartz sand from a marine pebble-cobble conglomerate at Walkerville North, 10 km NE of Cape Liptrap was dated at 132±9 ka by OSL and horizontal to wavy bedded fine-grained sands overlying a marine abrasion platform at Morgan's Beach was dated at 122±9 ka by OSL, both successions correlating with MIS 5e (Gardner et al., 2009). The lower terrace elevation at Morgan's Beach may be associated with down-faulting on the western side of a parallel trending fault, 2 km west of the Waratah Fault. Faulting and varied elevations of MIS 5e paleoshoreline successions

390 at Cape Liptrap suggest neotectonic motions since MIS 5e times, which is consistent with
391 seismic activity and the present-day stress field of Australia (Rajabi et al., 2017; Sandiford,
392 2003).
393
394 *2.1.8. Nature and basis for age of MIS 5e successions in New South Wales*
395 Although coastal barrier landforms are well-developed along sectors of the New South
396 Wales coastline, shell-rich, estuarine successions representing valuable paleosea level
397 information are less common due to removal of former interglacial sedimentary records by
398 fluvial erosion within confined bedrock valleys at times of low sea level (Nichol and Murray-
399 Wallace, 1992). Three critical sites for documenting relative sea level during MIS 5e in New
400 South Wales, include Gillard's Beach along the southern coastline (location 45; Young et al.,
401 1993), Largs, Hunter Valley (location 46; Murray-Wallace et al., 1996b; Thom and Murray-
402 Wallace, 1988) and Evans Head (location 47; Marshall and Thom, 1976). A relict cobble-
403 pebble beach facies at Gillard's Beach (location 45) yielded TL ages of 114±15 ka and 126±13
404 ka, indicating a relative sea level of up to 4.8 m APSL (Young et al., 1993). At Largs (location
405 46), an MIS 5e estuarine shell bed was deposited near the inland limit of a proto-estuary of the
406 Hunter River some 30 km inland from the present coastline (Thom and Murray-Wallace, 1988).
407 An MIS 5e age is based on AAR dating of *Anadara trapezia* and other fossil molluscs (Murray-
408 Wallace et al., 1996b). At Evans Head (location 47), fossil corals collected from an exposure
409 within a relict coastal barrier were dated at 114±9 to 127±18 ka, suggesting a paleosea level of
410 5±1 m APSL (Marshall and Thom, 1976).
411

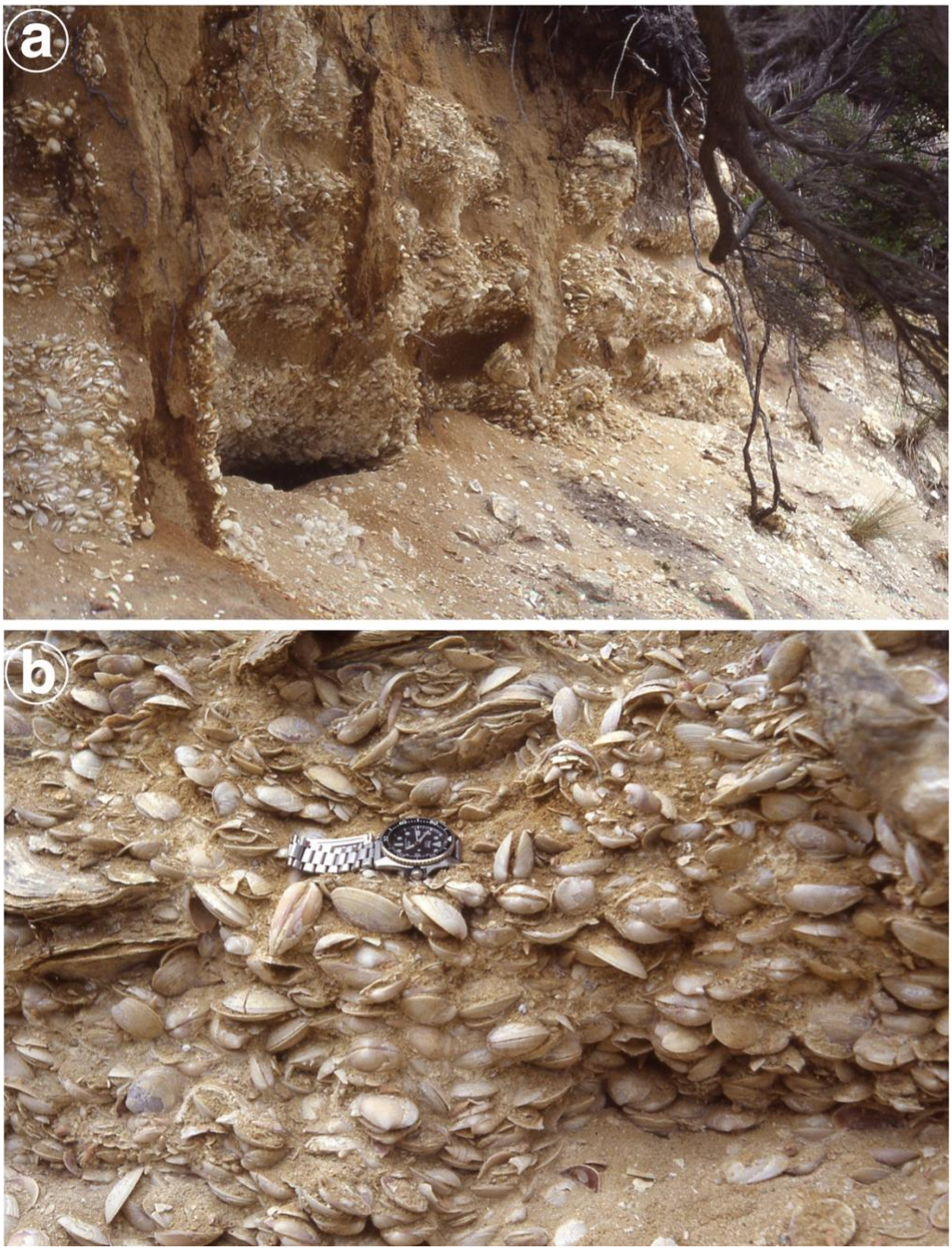

412

413 **Figure 7**. **a**. Last Interglacial (MIS 5e) estuarine-lagoonal sediments exposed in an eroding
414 embankment of the North East River, northern Flinders Island, Bass Strait, Tasmania (location
415 42). The three shelly successions (photographed in 1990) are dominated by abundant
416 articulated cockles in life position of the shallow water mollusc *Katelysia rhytiphora*
417 interbedded with depauperate sandy beds. *K. rhytiphora* lives gregariously in subtidal waters
418 immediately below low water datum and characteristically form coquina accumulations. The
419 upper bounding surface of the deposit is 4.5 m APSL. A Last Interglacial age has been
420 established by amino acid racemization and electron spin resonance dating (Murray-Wallace
421 and Goede, 1995). **b**. Detail of a portion of the lowest Last Interglacial shelly succession at
422 North East River, Flinders Island, Bass Strait, featured in **a**. The shelly succession (coquina) is
423 dominated by articulated and *in situ Katelysia rhytiphora* with five individuals of the oyster
424 *Ostrea angasi* also present, both species indicating shallow subtidal conditions at the time of
425 sedimentation.

426 *2.1.9. Nature and basis for age of MIS 5e successions in Tasmania*

427 Last interglacial (MIS 5e) coastal successions in Tasmania include a shallow water,
428 estuarine succession at Mary Ann Bay near Hobart (location 40; Fig. 5h-i), embayment fill
429 successions at Broadmeadows, Montagu and Mowbray Swamp (locations 36–38) on the north-
430 western coastline of the island, and a succession of relict beach ridges at Stumpys Bay (location
431 41) in north-eastern Tasmania (Bowden and Colhoun, 1984; Colhoun et al., 1982a; Murray-
432 Wallace and Goede, 1991; Murray-Wallace and Goede, 1995; Table 1). Last interglacial
433 successions on the Bass Strait Islands include successions at Yellow Rock River (location 34)
434 and Egg Lagoon (location 33) on King Island (Jennings, 1959; Murray-Wallace and Goede,
435 1995) and a succession in the North East River Estuary on Flinders Island (location 42;
436 Sutherland and Kershaw, 1971; Figs 5g and 7a-b). Coastal shingle deposits covered by
437 speleothems in relict sea caves at New River Lagoon, SW Tasmania, also attest to a higher
438 relative sea level during MIS 5e and local uplift since that time (Kiernan and Lauritzen, 2001).

439 Several lines of evidence led to a last interglacial age, being assigned provisionally to
440 these successions in Tasmania. The elevation of the successions above present sea level
441 (APSL) is generally too high for them to be regarded as Holocene (i.e. typically >11 m APSL).
442 In addition, radiocarbon ages for peat and marl that overlie marine shelly sands, and on fossil
443 molluscs from the coastal successions, yielded ages older than Holocene. In general,
444 radiocarbon dating of the Pleistocene materials yielded 'finite' ages close to the practical limits
445 of the radiocarbon method (Colhoun et al., 1982b; Gill and Banks, 1956; Van de Geer et al.,
446 1986). A minimum radiocarbon age of >52 ka (GrN-9743) on peat from Mowbray Swamp
447 (location 37) overlying fossiliferous, shallow marine sands in northwestern Tasmania (Van de
448 Geer et al., 1986) indicates that the previously reported 'finite' ages reflect contamination by
449 varying amounts of ^{14}C with a higher activity (yielding a younger apparent age) that could not
450 be removed during sample pre-treatment. Other evidence consistent with a Late Pleistocene

age centres on the morphostratigraphical, biostratigraphical and diagenetic character of the strata (Bowden and Colhoun, 1984) in conjunction with relative Late Quaternary glacio-eustatic sea-level change (Lambeck and Chappell, 2001).

A 9.6 m thick succession of tabular cross-stratified shelly sands rests unconformably on an eroded bench of Jurassic dolerite at Mary Ann Bay (location 40), adjacent to the Derwent Estuary in south-eastern Tasmania (Fig. 5h-i). The mollusc-rich succession has long been the subject of interest in view of its physical setting, which extends up to 24.5 m APSL, and is accordingly significant in terms of the relative sea level and neotectonic history of the region (Bowden and Colhoun, 1984; Lambeck and Chappell, 2001; Murray-Wallace and Goede, 1991; Murray-Wallace and Goede, 1995; Van de Geer et al., 1986). The shelly sands contain 49 species of fossil marine molluscs (Colhoun et al., 1982a; Slee et al., 2012), many of the species signifying shallow water deposition in an estuarine environment similar to the modern Derwent Estuary. A Last Interglacial age (MIS 5e) for these shelly successions has been established based on AAR and ESR dating of the marine molluscs *Fulvia tenuicostata*, and *Pecten meridionalis* (Murray-Wallace and Goede, 1991; Murray-Wallace and Goede, 1995; Slee et al., 2012).

A spectacular succession of relict foredunes (beach ridges) is preserved on Remarkable Banks, a coastal plain trending NNE on Robbins Island (location 35), northwestern Tasmania (Bowden and Colhoun, 1984; Goodwin et al., 2023). Minimal erosional truncation of individual ridges, reflecting a relatively low energy depositional environment has also preserved the seaward intertidal facies for each ridge, critical for paleosea level interpretations (Goodwin et al., 2023). The progradational sequence of approximately 140 relict foredunes grade from 11 m to 4 m APSL across a 7 km long coastal plain, with OSL ages ranging seawards from 130.3 to 117.5 ka for the relict foredunes (Goodwin et al., 2023). Relative sea level during this period is represented by three discrete phases: sea level fall from 7 m to 6 m

476 APSL between 130–126 ka, a stillstand at 5.75 ± 0.5 m APSL from 126–121 ka, and a fall in
477 sea level between 119–114 ka (Goodwin et al., 2023). The Robbins Island MIS 5e sea level
478 history is important for its longer time-series record than available from many other sites in
479 southern Australia. Notably, the beach ridge succession does not record the higher MIS 5e
480 relative sea levels documented from mainland Tasmania (Murray-Wallace et al., 1990; Murray-
481 Wallace and Goede, 1991; Murray-Wallace and Goede, 1995).
482
483 **2.2 MIS 5e sea surface from paleoshoreline elevations**
484 The Last Interglacial coastal sedimentary record of southern Australia is fragmentary, with
485 most successions preserving a more limited portion of the interglaciation. Fewer examples of
486 relatively complete records, spanning the interval 128–116 ka have been identified. In broad
487 view, the MIS 5e Glanville Formation in South Australia is 1–3 m thick (Belperio et al., 1995;
488 Murray-Wallace et al., 2016; Pan et al., 2018). The upper bounding surface of the formation is
489 defined by pedogenic calcrete, resulting from subaerial exposure of the coastal successions
490 accompanying a fall in sea level (forced regression) at the end of MIS 5e. Although the upper
491 bounding surfaces of all the MIS 5e sedimentary units reported in this study signify a cessation
492 in deposition, it is unlikely that they represent substantial deflation surfaces, as the thickness
493 of the sedimentary successions are marine limited, having been defined by a common elevation
494 of paleosea level during MIS 5e, and regionally, a common thickness of the formations is noted.
495 Based on global records of Late Quaternary sea-level changes, all the successions reported
496 here, have remained above sea level since the end of MIS 5e (Murray-Wallace and Woodroffe,
497 2014). The calcrete profiles on the Glanville Formation suggest limited erosion and exhumation
498 of the primary sedimentary units, notwithstanding that they might not originally have
499 represented the entire interglacial sea level highstand. Accordingly, surface uplift mostly

500 represents rock (crustal) uplift of much of the original sedimentary units (England and Molnar,
501 1990).

502 Most of the Last Interglacial successions reported in this investigation record deposition
503 since the culmination of sea-level rise in the early portion of MIS 5e. Exceptions include the
504 Woakwine Range in South Australia, which chronicles the latest portion of sea-level rise and
505 a falling stage sea level during the interglacial, possibly linked to hydro-isostasy (Murray-
506 Wallace et al., 1999). The upward deepening succession at Point Turton, southern Yorke
507 Peninsula (location 12), also documents a relative sea-level rise during MIS 5e without
508 evidence for two sea level highstands (Pan et al., 2018). The prograded beach ridge plain on
509 Robbins Island also records relative sea-level changes during MIS 5e from c. 129–114 ka
510 (Goodwin et al., 2023).

511
512 *2.2.1. Basis for relative sea-level observations from the sedimentary facies*

513 In this work, relative paleosea levels (Table 1) have been determined primarily from
514 sedimentary lithofacies and their contained molluscan faunal assemblages, particularly where
515 species occur within a narrow range of tidal datum. Molluscan species identification follows
516 Ludbrook (1984). Characteristic sedimentary facies from which paleosea level has been
517 determined include beach (lower foreshore), and back-barrier estuarine-lagoonal facies.
518 Paleosea levels have been inferred based on the location and elevation of sea-level indicators
519 and their relation to a former tidal datum at the time of sedimentation (sea-level index point
520 sensu Shennan, 2015 and Rovere et al., 2023). Accordingly, modern tidal ranges across the
521 field sites were considered in the determination of paleosea level.

522 Beach facies (lower foreshore) represented by planar cross-bedded bioclastic sands
523 containing the cockle *Donax deltoides* are common along the open ocean coastlines of
524 southeastern Australia. In modern environments, the infaunal species characteristically
525 burrows to 5–10 cm below the sediment-water interface of foreshore sediments and repeatedly

emerge and reburrow in the lower intertidal sands up to 20 cm below present sea level (Prezant, 1998). *Donax deltoides* migrate laterally within the sediment profile in response to tidal movements but remain within the swash-zone and are most abundant just below low tide level and may indicate a paleosea level within a range of ±0.5 m

The estuarine mollusc *Anadara trapezia* is a shallow-burrowing bivalve of semi-infaunal habit found on the surfaces of tidal flats within estuaries with good tidal exchange of waters (Murray-Wallace et al., 2000). The cockle *Katelysia* spp. occurs within many of the Last Interglacial estuarine successions of southeastern Australia as coquina accumulations of shells (Fig. 7). In modern environments, the genus occurs abundantly in protected, intertidal sandflats representing the dominant mollusc (Harte, 1998; Ludbrook, 1984). *Katelysia scalarina* characteristically occurs in intertidal to shallow subtidal habitats, while *Katelysia rhytiphora* tends to frequent shallow subtidal waters immediately below low water limit of the intertidal zone to a depth of approximately 1 m below low tidal datum (Nielsen, 1964; Roberts, 1984). The turreted gastropod *Batillaria* (*Zeacumantus*) *diemenensis* is also common in the Last Interglacial successions of southeastern Australia. The species grazes just below the sediment-water interface on sand and mud flats and occurs most prolifically in intertidal environments (Ludbrook, 1984; Macpherson and Gabriel, 1962).

2.2.2. Regional dataset

The age, spatial distribution, and paleosea levels inferred from Last Interglacial coastal landforms and sedimentary successions in southeastern Australia, have been sufficiently well-defined that their wider significance for understanding the long-term behaviour of the lithosphere-mantle couplet and its role in geodetic changes since MIS 5e can be undertaken.

MIS 5e shoreline elevations and paleosea levels from southeastern Australia were compiled from 47 locations (Fig. 1 and Table 1). The age uncertainty of the data is generally in the order of ±2–3 ka for uranium-series ages by MC-ICP-MS, and up to ±10 ka for earlier

551 measurements by α-counting. Luminescence ages typically have uncertainties ranging from ±5
552 to ±10% (±4–11 ka), that increase with age (see Table 6.1 in Murray-Wallace, 2018).
553 Uncertainties in inferred paleosea levels vary with the reliability of paleosea level indicators
554 but are generally in the range of ±0.5–1 m (Table 1). The inferred vertical surface displacement
555 *SD* (m) of the relict shoreline successions is taken as $SD = h + WD - SL$, where h is the
556 maximum elevation of the shoreline succession, *WD* the paleowater depth and *SL* is the
557 elevation of the MIS 5e sea surface in this remote, far-field region. A value of 4±1 m APSL is
558 adopted, based on the paleosea-level observations from western Eyre Peninsula, and southern
559 Yorke Peninsula, part of the tectonically highly stable Gawler Craton in South Australia
560 (Murray-Wallace et al., 2016; Pan et al., 2018; see Section 3.1). Uncertainties associated with
561 WD and SL were propagated as $E = \sqrt{e_{\mathrm{h}}^2 + e_{\mathrm{WD}}^2 + e_{\mathrm{SL}}^2}$, where e_{h} = 0.05 m (except for the New
562 River Lagoon Sea Caves, SW Tasmania, for which it was equal to one metre) was the
563 uncertainty associated with present-day elevation, e_{WD} was the uncertainty associated with
564 paleosea level (Table 1) and e_{SL} = 1 m was the uncertainty associated with global sea level
565 (Fig. 8b).
566
567 **2.3. Geological and geophysical data**
568
569 Topographical relief was based on continental-scale digital elevation models with
570 resolution ~435 m (GA, 2019) and regional-scale models with resolution ~30 m (JPL, 2013).
571 The location and magnitude of 416 earthquakes between 1973 and 2024 with magnitudes
572 greater than 2.5 were obtained from the Geoscience Australia Earthquake Catalogue (GA,
573 2024) on 9 September 2024. The magnitude of events was defined using either Richter
574 magnitude (282 events), body wave magnitude (129 events), moment magnitude (four events),
575 or coda magnitude (one event).

Quaternary volcanic formations were represented at the 1:1 million scale (GA, 2012), faults at the 1:2.5 million scale (Raymond, 2023), and the Gawler Craton and Adelaide Fold Belt at the 1:5 million scale (Blake, 1998). The upper surface of the Oligo-Miocene Gambier Limestone was digitised from Figure 4.9 of Murray-Wallace (2018), and the outline of the Mount Gambier uplift was digitised from Figure 9 of Sprigg (1952). Reconstructions of the Cosgrove hotspot track by Davies et al. (2015) and by Seton et al. (2019) were obtained from the corresponding authors of these articles.

Continental crustal thickness was represented by an interpolated discrete global model (Stephenson et al., 2024) at 0.25 degree resolution. Lithospheric thickness was represented using the model of Hoggard et al. (2020), residual topography using the model of Stephenson et al. (2024) and dynamic topography using the model of Davies et al. (2019) that considers the structure of the lithosphere. Sub-lithospheric mantle structure was based on tomographic models PRI-S05 (Montelli et al., 2006), REVEAL (Thrastarson et al., 2024) and UU-P07 (Amaru, 2007).

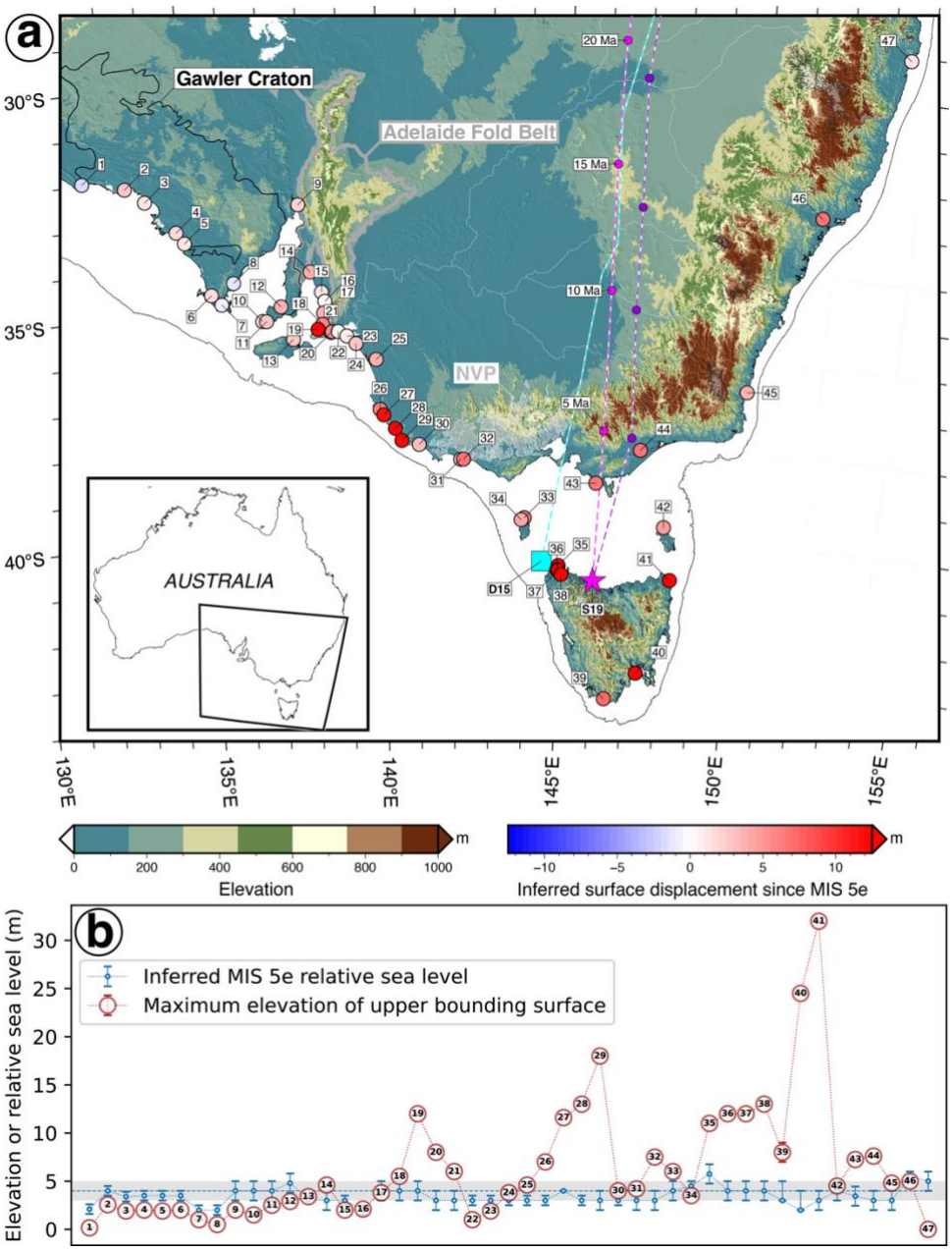

Figure 8. Inferred surface displacement of Last Interglacial shoreline successions in southeastern Australia. a, Digital Elevation Model (GA, 2019) and Last Interglacial shoreline successions at 47 locations (Table 1), shown as disks coloured by inferred surface displacement assuming sea level was 4 m higher during the Last Interglacial. Quaternary volcanic formations (GA, 2012) are shown as transparent grey polygons with a white outline, and earlier Cenozoic volcanic formations are shown as transparent grey polygons with a black outline. The reconstructed Cosgrove hotspot track is shown as a cyan dashed line and a cyan square labelled 'D15' for the inferred present-day location based on the original publication (Davies et al., 2015), and as magenta and purple dashed lines for two alternative reconstructions by Seton et al. (2019), ending at the inferred present-day location shown as a magenta star labelled 'S19'. Light shading from azimuth 225º. **b-c**, Present-day maximum elevation and inferred paleowater depth for the considered MIS 5e paleoshoreline successions. The dashed line indicates a MIS 5e sea level 4 m higher than present-day for southern Australia (Murray-Wallace et al., 2016; Pan et al., 2018), with an uncertainty of ± 1 m (grey polygon). 'NVP': Newer Volcanics

Province. The Gawler Craton and Adelaide Fold Belt at the 1:5 million scale (Blake, 1998) are shown as grey polygons. The inset shows the map area in the context of Australian coastlines.

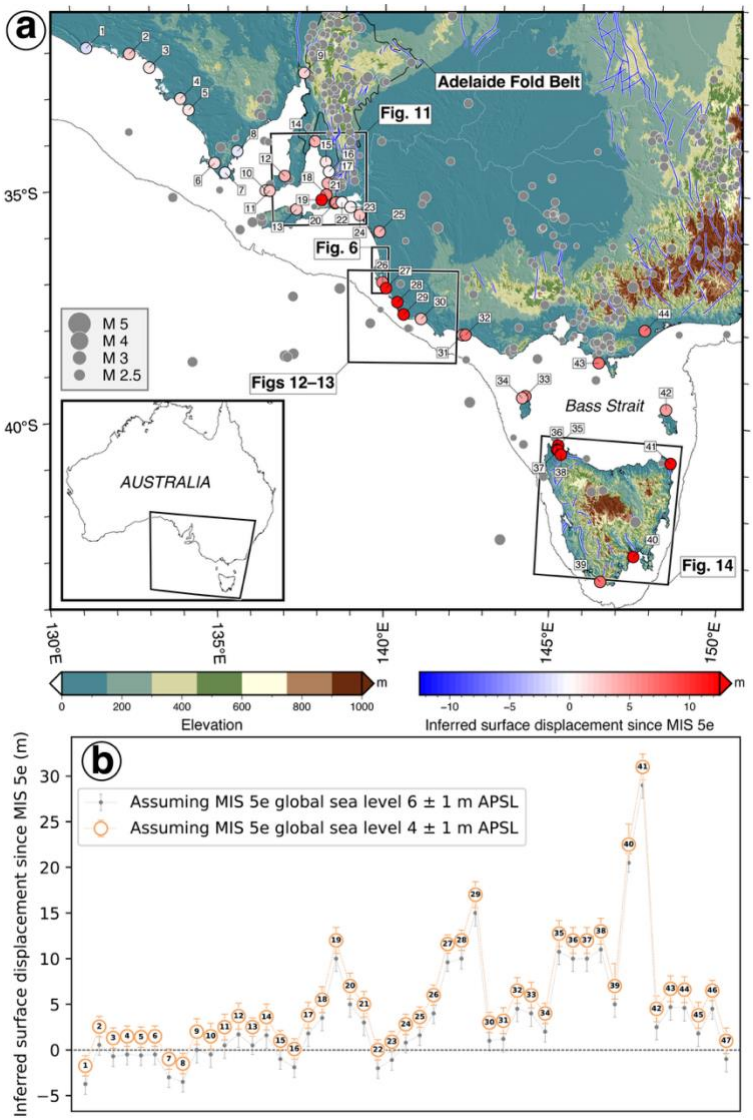

Figure 9. Inferred surface displacement of Last Interglacial shoreline successions, earthquakes, and major faults in southeastern Australia. a, Digital Elevation Model (GA, 2019) and Last Interglacial shoreline successions at 44 locations (Table 1), shown as disks coloured by inferred surface displacement assuming a 4 m higher sea level during MIS 5e than in the current, Holocene Interglacial. Earthquakes (GA, 2024) are shown as grey disks sized according to magnitude, and major faults (Raymond, 2023) are shown as blue lines. Light shading from azimuth 225º. **b**, Inferred surface displacement at all 47 considered locations assuming MIS 5e global sea level to have been either 4 ± 1 m or 6 ± 1 m above present-day sea level (APSL).

3. Analysis

3.1. MIS 5e sea level in southern Australia and globally

MIS 5e ice-equivalent sea level relative to present-day for southern Australia has been documented at between 2.1 ± 0.5 m APSL (Fowlers Bay, location 1), at 4 ± 0.5 m APSL (Tourville Bay, location 2), Eyre Peninsula (Murray-Wallace et al., 2016) and at 4.8 ± 1 m APSL at Point Turton, Hardwicke Bay, southern Yorke Peninsula (location 12). Based on these estimates, and on the average paleosea level for the considered sites is ~3.5 ± 0.7 m (Table 1), a 4 ± 1 m APSL value for a MIS 5e sea surface is adopted in this study for southeastern Australia (Fig. 8b). Although this suggested MIS 5e sea surface is below the proposed global mean MIS 5e sea level of between 6–9 m APSL (Dutton et al., 2015), the southern Australian observations are more representative of an ice-equivalent sea level with limited postglacial adjustment in this remote far-field region from former Pleistocene ice sheets (Conrad, 2013).

Uplift by more than 10 m since MIS 5e was inferred at ten locations (Figs 8-9), six of which are in Tasmania (locations 35–38 and 40–41), three on the Coorong Coastal Plain between Robe and Mount Gambier (locations 27-29), and one at Normanville, southern Fleurieu Peninsula (location 19, Fig. 1). Subsidence by less than 2 m (Figs 8-9) since MIS 5e times was inferred for Fowlers Bay, Port Lincoln, and Tumby Bay (locations 1, 7, and 8), all of which occur west of 139ºE and north of 35.6ºS, in the Gawler Craton (Figs 8-9).

Inferred surface displacement since MIS 5e tended to increase towards the east (Fig. 10a) and towards the south (Fig. 10b), as shown using Spearman's rank correlation coefficient, which assesses the monotonic relationship between two ranked variables (Spearman, 1904). There were statistically significant Spearman ranking correlations between inferred surface displacements since MIS 5e and latitude (r = 0.74, Fig. 10b) as well as longitude (r = 0.63, Fig. 10a).

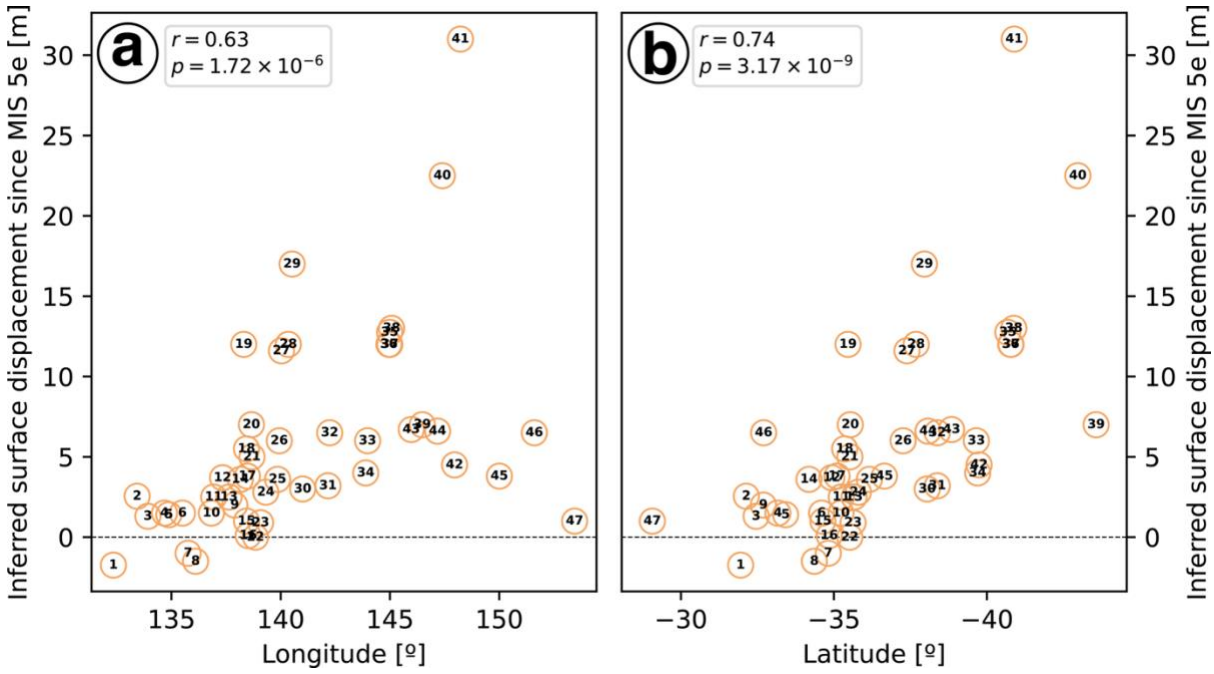

651

652 **Figure 10.** Inferred surface displacement of paleoshoreline successions since MIS 5e as a
653 function of longitude (**a**) and latitude (**b**). *r* is the Spearman correlation coefficient, and *p* is the
654 *p*-value for a Spearman ranking test with null hypothesis that two samples have no ordinal
655 correlation.

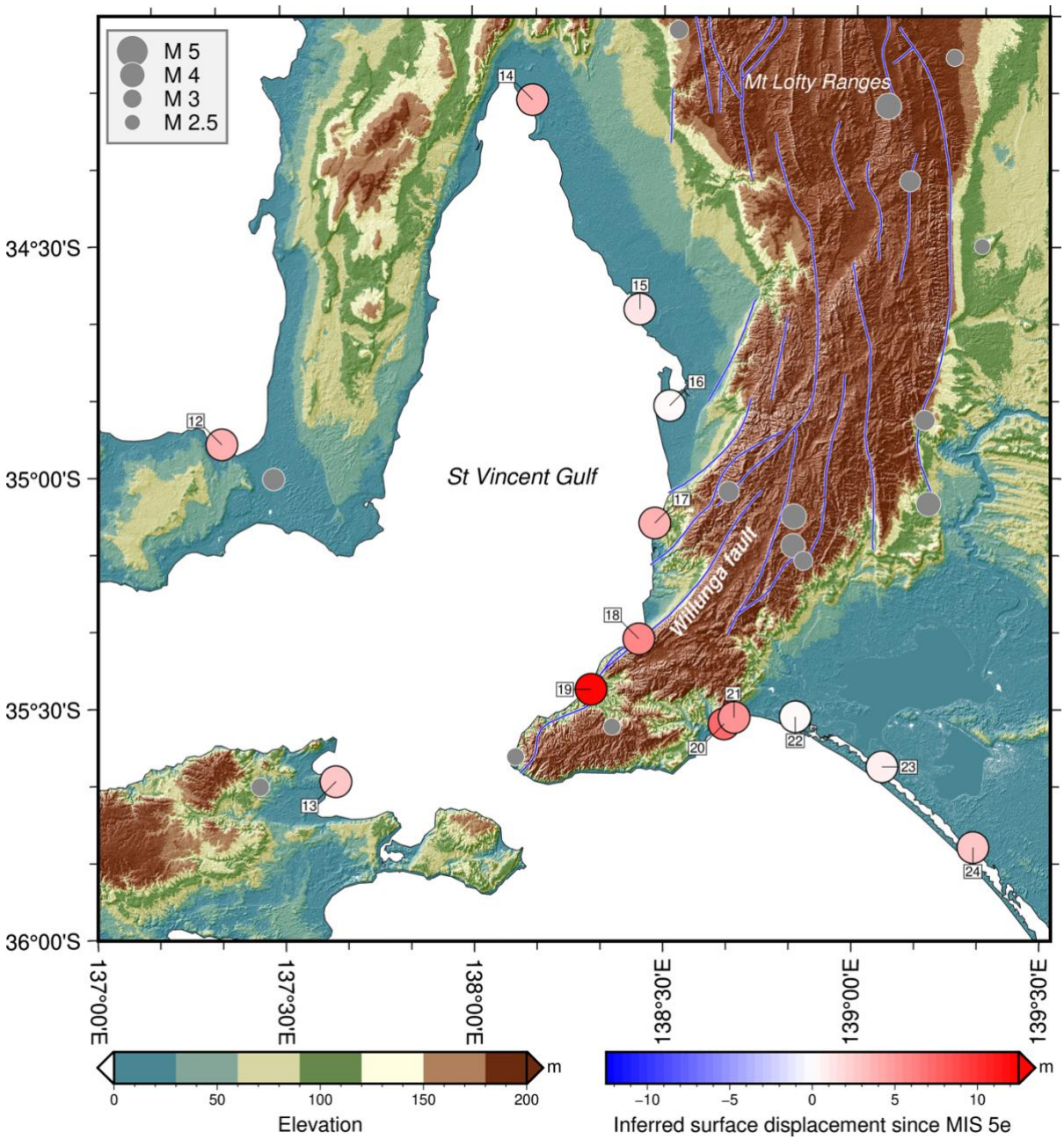

Figure 11. Inferred surface displacement of Last Interglacial shoreline successions, earthquakes, and major faults around Gulf St Vincent, Fleurieu Peninsula and the northern Coorong Coastal Plain. Digital Elevation Model (JPL, 2013) and Last Interglacial coastal successions at 13 locations (Table 1), shown as disks coloured by inferred surface displacement assuming a 4 m APSL sea level during the Last Interglacial (MIS 5e). Earthquakes (GA, 2024) are shown as grey disks sized according to magnitude, and major faults (Raymond, 2023) are shown as blue lines. Light shading from azimuth 315º. The region is outlined in Figure 9a.

669 **3.2.Tectonic setting**

670 Southeastern Australia consists of several geotectonic provinces defined based on their
671 distinctive bedrock and structural characteristics, tectonic history, and regional assemblages of
672 landforms (Murray-Wallace, 2002; Preiss et al., 2002). The Gawler Craton extends across the
673 western study area, covering all of Eyre Peninsula, Spencer Gulf and Yorke Peninsula. The
674 regional bedrock has been tectonically stable since the last deformation event 1.5 Ga ago
675 (Fanning et al., 2007; Preiss et al., 2002). The low relief, gently undulating landscapes of the
676 Gawler Craton have developed on late Archean greenstone belts, high-grade metamorphic
677 rocks and felsic volcanics, and Paleoproterozoic and early Mesoproterozoic orogenic belts
678 subjected to deformation and magmatism (Preiss et al., 2002). The inferred surface
679 displacement since MIS 5e at locations in the Gawler Craton region (1-8 and 10-12, Figs 1, 8-
680 9) is within -2 m and +4 m (Fig. 9b), which suggests continued stability of the Gawler Craton
681 since MIS 5e, with local post-depositional subsidence at Fowlers Bay, Port Lincoln, and
682 Tumby Bay (locations 1, 7, and 8) possibly due to hydro-isostasy during the sea level highstand
683 of MIS 5e as noted in the current Holocene Interglacial (Belperio et al., 2002). It is also possible
684 that paleoshoreline successions reflecting minor subsidence represent only the latter, lower sea
685 level portion of MIS 5e highstand, implying that a MIS 5e sea level highstand of lower than
686 4 m APSL is more appropriate to infer vertical displacement at these locations.

687 The eastern boundary of the Gawler Craton corresponds with the Torrens Hinge Zone,
688 which defined a transitional area of rifting from the craton to the Adelaide Rift Complex
689 (formerly termed Adelaide Geosyncline) during its depositional history (Preiss et al., 2002).
690 The elongate, north-south trending upland region of the Mount Lofty and Flinders Ranges,
691 defines the limit of a fault-bound, deeply eroded Neoproterozoic–Cambrian age fold belt. The
692 eastern margin of Eyre Peninsula, Spencer Gulf, Yorke Peninsula, Gulf St Vincent, and the
693 Mount Lofty and Flinders Ranges are fault-bound landscapes with notable seismic activity

694 along the regional faults that define these features (Fig. 11). The gulfs, peninsulas and the
695 Mount Lofty and Flinders Ranges, represent graben and horst structures respectively. Faults
696 and earthquakes represented at the regional scale reveals that the most significant seismicity
697 occurs in the Adelaide Fold Belt, with some activity in the southeastern part of the mainland
698 (Fig. 9a), which is well established (e.g., Rajabi et al., 2017; Sandiford, 2003). Around Gulf St
699 Vincent (Fig. 11), inferred surface displacement since MIS 5e range between 0 m and 12 m
700 (average ~3.7 m) with Normanville standing out and well above the range at Normanville
701 (location 19, 12 m). Both Sellicks Beach and Normanville (locations 18 and 19) are close to
702 the Willunga Fault. The difference in inferred surface displacement since MIS 5e between these
703 two locations suggests up to 6.5 m of upward displacement of the block to the southeast of the
704 Willunga Fault (Fig. 11). Chiton Rocks and Victor Harbor (locations 20 and 21) are in the
705 foothills of the southern Mount Lofty Ranges on Fleurieu Peninsula, and close to the
706 seismically active Adelaide Fold Belt (Figs 9 and 11), suggesting that the modest inferred uplift
707 they experienced (7 m and 5 m, respectively) could also be affected by neotectonic motions.
708
709

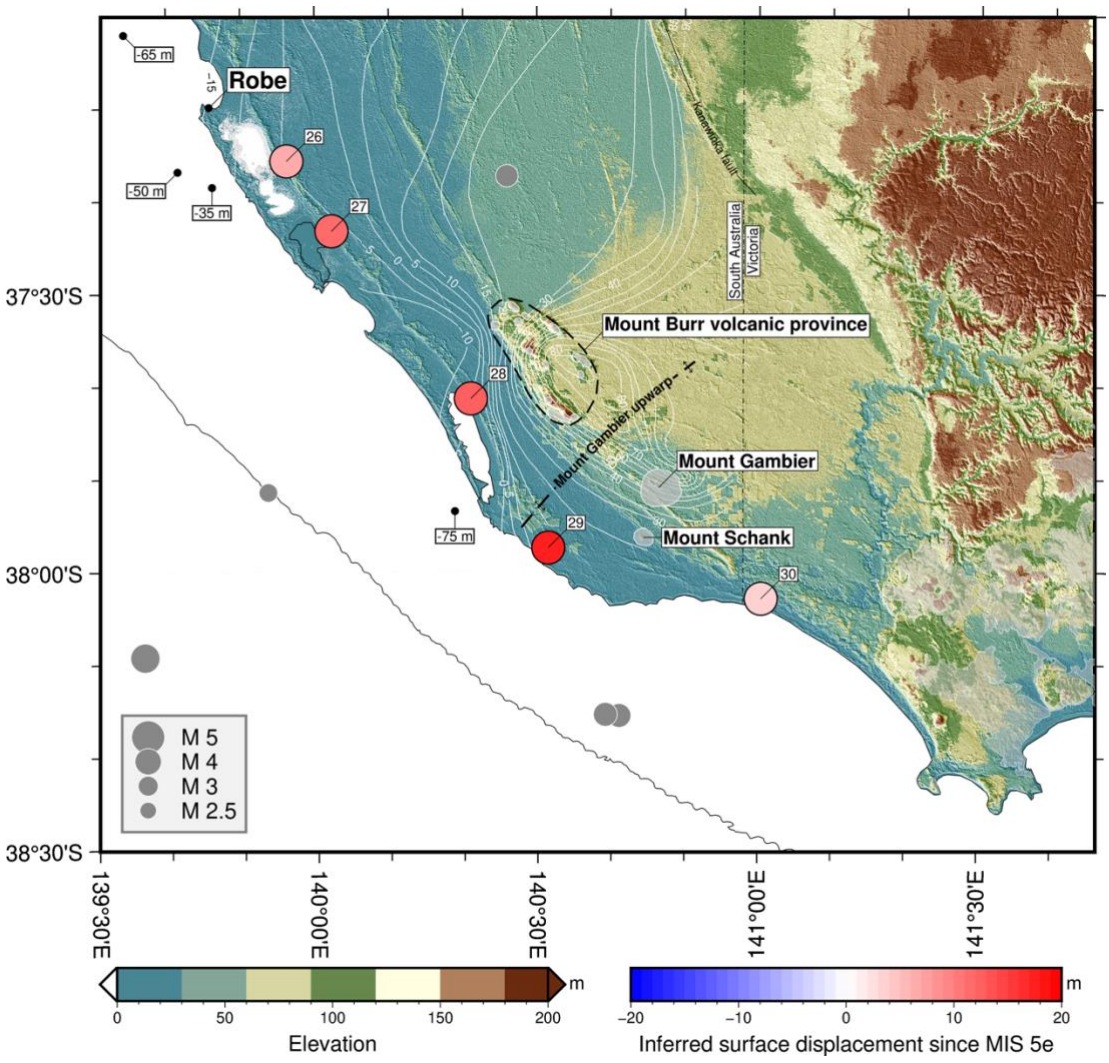

Figure 12. Inferred surface displacement of Last Interglacial shoreline successions, earthquakes, and Quaternary volcanic formations between Robe and Mount Gambier. a, Digital Elevation Model (JPL, 2013) and Last Interglacial successions at five locations (Table 1), shown as disks coloured by inferred surface displacement assuming a 4 m APSL sea level during the Last Interglacial (MIS 5e). Quaternary volcanic formations (GA, 2012) are shown as transparent grey polygons with a white outline. White contours show the upper bounding surface of the Oligo-Miocene Gambier Limestone, with offshore values indicating the depth of the Gambier Limestone below present-day sea level. Light shading from azimuth 225º. The region is outlined in Figure 9a.

The Paleogene–Neogene Murray Basin is an epicratonic marine basin immediately to the east of the Mount Lofty Ranges. The basin fill was initiated some 45 Myr ago during the separation of Antarctica and southern Australia. The Murray Lakes (lakes Alexandrina and Albert) and River Murray mouth area, adjacent the Mount Lofty Ranges, is a zone of subsidence in the southwestern Murray Basin in response to sediment accumulation within the

727 failed delta area of the River Murray (Murray-Wallace et al., 2010) and uplift farther north
728 associated with reverse faulting of Cambrian Kanmantoo metasedimentary rocks over Miocene
729 limestones and Quaternary fanglomerates on the Millendella Fault (Bourman and Lindsay,
730 1989). Epeirogenic uplift involving differential tilting is evident across the Coorong Coastal
731 Plain as shown by an emergent series of interglacial coastal barriers having formed over the
732 past 1 Myr (Murray-Wallace, 2018). Uplift by more than 10 m since MIS 5e times was inferred
733 in the vicinity of Quaternary volcanic formations, some 45 km to the west of the Newer
734 Volcanic Province (Figs 8a and 12). The inferred uplift increases from west to east between
735 Lake Hawdon South (location 26) and Nene Valley (location 29) from 6 m to 17 m over
736 120 km, then decreases down to 3 m at Nelson (location 30) over approximately 40 km (Figs 8a
737 and 12). This increase by ~11 m between Lake Hawdon South and Nene Valley along the
738 Woakwine Range generally reflects the increase in the elevation of the upper-bounding surface
739 of the Oligo-Miocene Gambier Limestone by < 19 m between these locations, which is
740 associated with the upwarp of the Gambier Limestone in a dome structure around Mount
741 Gambier (Sprigg, 1952; Fig. 12). Given their spatial association with volcanic formations, the
742 Gambier upwarp and the trend in inferred uplift since MIS 5e are likely due to crustal doming
743 in response to shallow emplacement of magma at the Mount Burr Volcanic Complex during
744 Pleistocene times and at Mount Gambier and Mount Schank during Holocene times.
745 The Pleistocene Mount Burr Volcanic Complex represented an archipelago of volcanoes,
746 with the western most centres showing evidence of erosional modification during sea level
747 highstands and the deposition of calcarenite (aeolianite) of the Lower Bridgewater Formation
748 on the slopes of Mounts Graham, Muir, MacIntyre and Burr (Hossfeld, 1950; Sprigg, 1952). A
749 cuspate foreland developed, extending from the West Naracoorte Range (MIS 21-19) to the
750 Mount Burr Volcanic Complex. The coastal barriers Harper Range and Stewarts/Cave Range

751 nucleated against the volcanic centres commencing at least, some 700 ka ago (MIS 17)
752 indicating a minimum age for the volcanism (Murray-Wallace, 2018; Fig. 13).
753

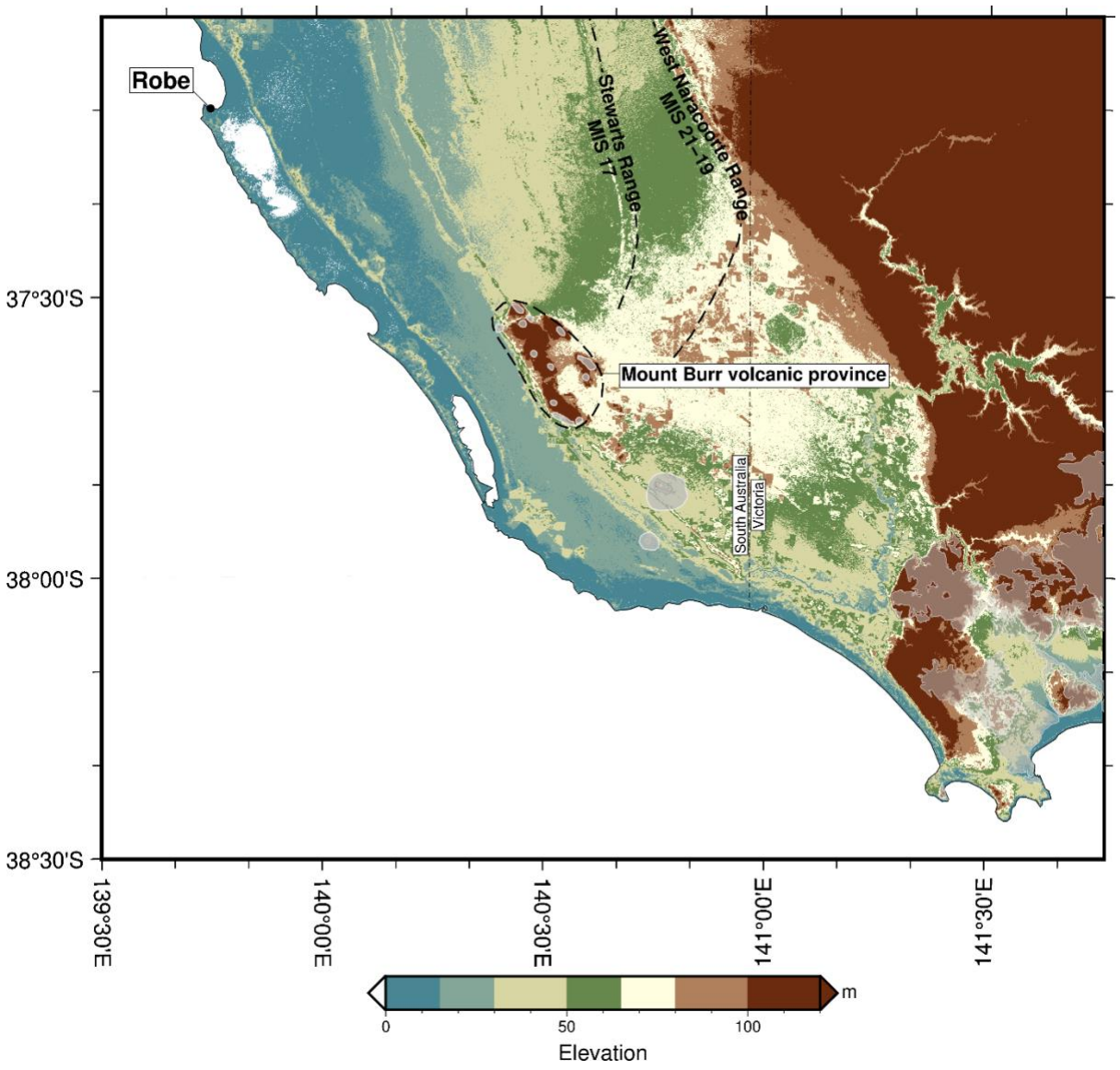

754

755 **Figure 13. Inferred minimum age of the Mount Burr volcanic province.** Digital Elevation
756 Model (JPL, 2013) with Quaternary volcanic formations (GA, 2012) shown as transparent grey
757 polygons with white outlines. The Naracoorte Range (MIS 21-19) and Stewarts Range
758 (MIS 17) are highlighted. Their cuspate shape suggest that they nucleated on the Mount Burr
759 volcanic province, which can be inferred to date back to MIS 17 times (~700 ka). Light shading
760 from azimuth 225º. The region is outlined in Figure 9a.

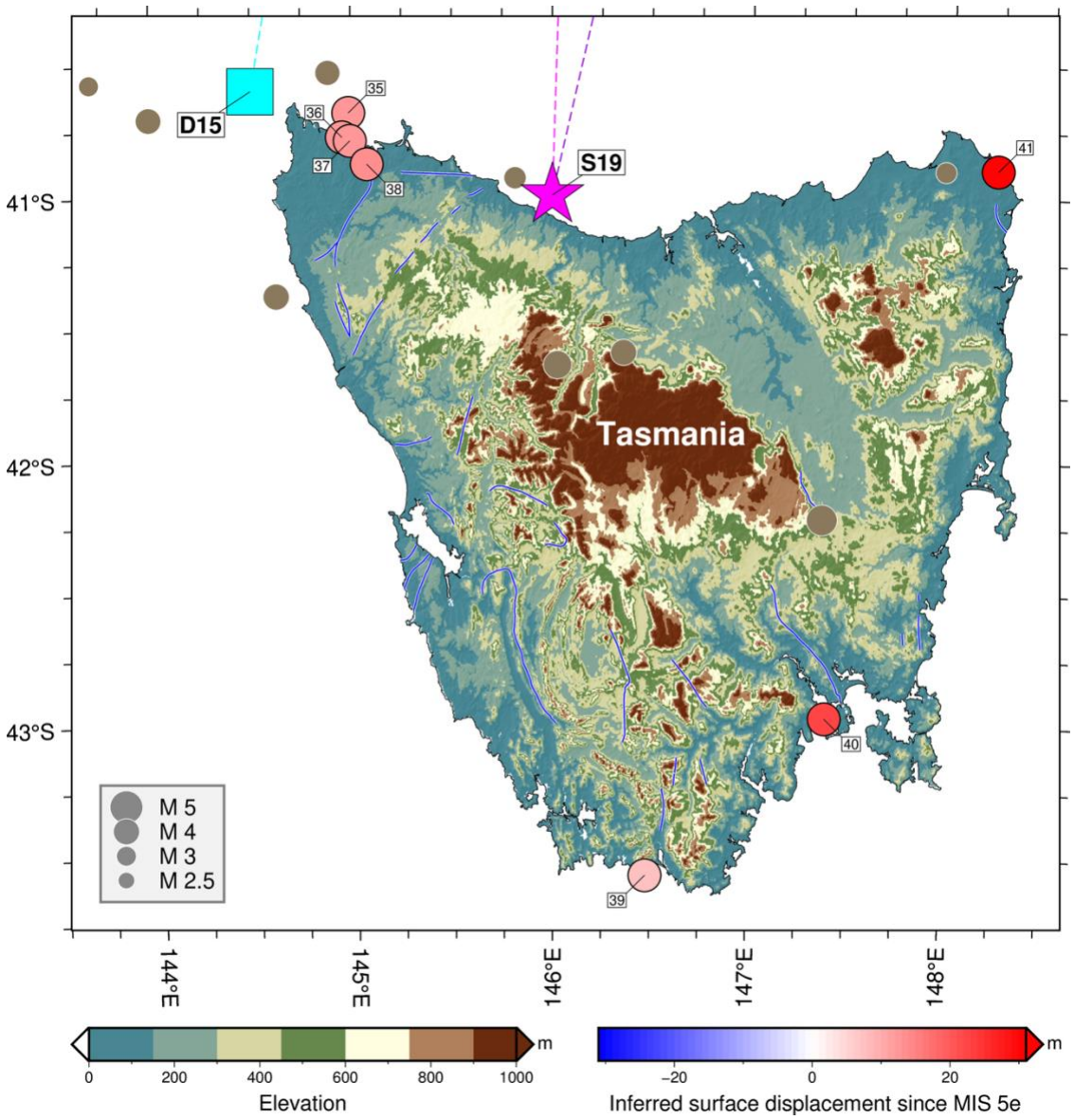

Figure 14. Inferred surface displacement of Last Interglacial shoreline successions, earthquakes, and major faults in Tasmania. Digital Elevation Model (GA, 2019) and Last Interglacial shoreline successions at seven locations (Table 1), shown as disks coloured by inferred surface displacement assuming a 4 m APSL sea level during MIS 5e. Earthquakes (GA, 2024) are shown as brown disks sized according to magnitude, and major faults (Raymond, 2023) are shown as blue lines. The reconstructed Cosgrove hotspot track is shown as a cyan dashed line and a cyan square labelled 'D15' for the inferred present-day location based on the original publication (Davies et al., 2015), and as magenta and purple dashed lines for two alternative reconstructions by Seton et al. (2019), ending at the inferred present-day location shown as a magenta star labelled 'S19'. Light shading from azimuth 315º. The region is outlined in Figure 9a.

The Lachlan Fold Belt (Cambrian to Early Carboniferous), Sydney Basin (Late Carboniferous to Middle Triassic) and New England Fold Belt (Silurian to Triassic) encompass the region from western Victoria to northern New South Wales and define the northern limit

778 of this investigation. Collectively, these regions confer a high degree of tectonic stability to the
779 coastal landscapes developed within these geotectonic provinces, as illustrated by the absence
780 of emergent shoreline complexes. Although the pre-Quaternary bedrock of Tasmania is related
781 to the eastern mainland of Australia (e.g. Lachlan Fold Belt), Last Interglacial coastal
782 successions occur at higher landscape elevations in Tasmania (Bowden and Colhoun, 1984;
783 Murray-Wallace and Goede, 1991; Murray-Wallace and Goede, 1995). Indeed, the inferred
784 uplift since MIS 5e times is largest in Tasmania (between 7 m and 31 m on the main island),
785 in the absence of Quaternary volcanic activity or of significant seismic activity (Figs 8, 9, and
786 14).
787
788 **3.3. Geodynamic setting**
789 3.3.1. Seismic tomography
790 A geodynamic process that does not result in seismicity or volcanism should explain the
791 uplift inferred since MIS 5e for Tasmania. Tasmania is at the end of the Cosgrove hotspot track,
792 with reconstructions by Davies et al. (2015) and Seton et al. (2019) both predicting the present-
793 day location of the hotspot to be just offshore and to the northwest (D19) or north (S19) of the
794 main Tasmanian island, respectively. This suggests that active mantle upwelling could be the
795 driver for the uplift of Tasmania by 7 m to 31 m since MIS 5e times. Some seismic tomographic
796 models suggest that seismic waves propagate more slowly through the mantle beneath
797 Tasmania (Figs 15-17), which implies that the mantle is hotter. This feature is most prominent
798 in seismic tomographic model PRI-S05 (Montelli et al., 2006), which was designed to image
799 mantle plumes. In that model, there is a clear slow S-wave velocity (V_S) anomaly at 200 km
800 depth centred beneath the northeastern part of Tasmania, which coincides with the largest
801 inferred uplift since MIS 5e at Stumpys Bay (31 m, location 41, Figs 8b, 9b, 14 and 15b). The
802 anomaly appears to extend between ~100 km and ~500 km depths, and it is most prominent

between ~200 km and ~400 km depth (Fig. 15b-e). The *Vs* anomaly is most pronounced and shallowest beneath Stumpys Bay, and less pronounced and deeper beneath Mary Ann Bay (location 40, inferred uplift: 22.5 m).

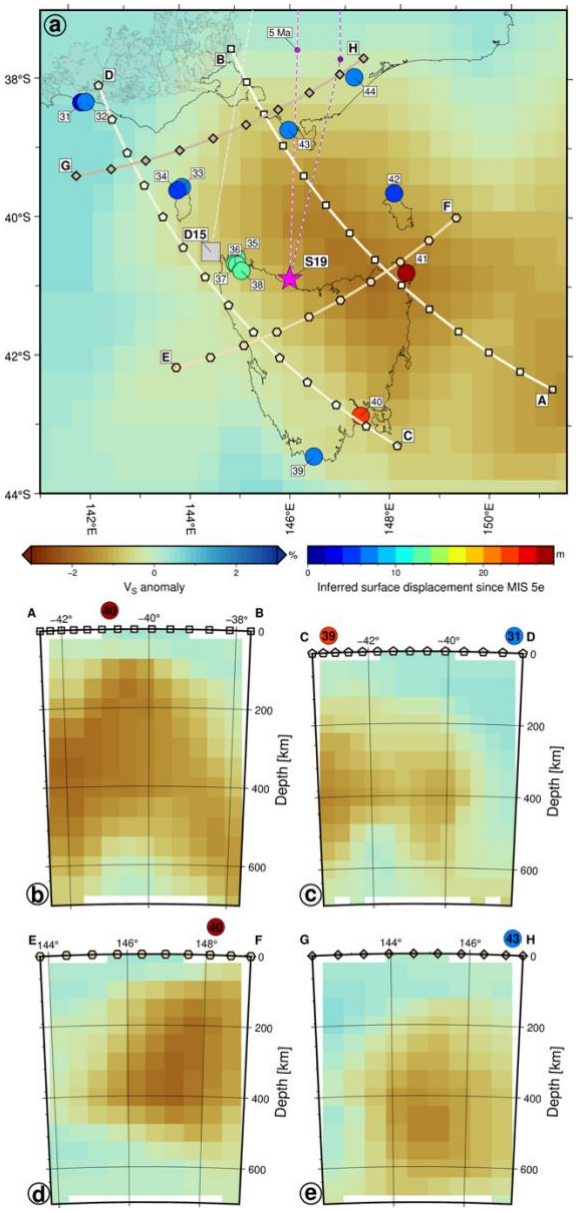

Figure 15. Inferred surface displacement of Last Interglacial shoreline successions and seismic tomography. a, Seismic tomography model PRI-S05 (Montelli et al., 2006) at 200 km depth, and Last Interglacial shoreline successions at 14 locations (Table 1) shown as disks coloured by inferred surface displacement assuming a 4 m APSL sea level during MIS 5e. Quaternary volcanic formations (GA, 2012) are shown as transparent grey polygons with a black outline. The reconstructed Cosgrove hotspot track is shown as a cyan dashed line and a grey square labelled 'D15' for the inferred present-day location based on the original publication (Davies et al., 2015), and as magenta and purple dashed lines for two alternative

reconstructions by Seton et al. (2019), ending at the inferred present-day location shown as a magenta star labelled 'S19'. Cross-sections along small circles A-B, C-D, E-F, and G-H are shown with symbols matching panels **b-e.** Cross-sections of seismic topography model PRI-S05 down to 700 km depth along small-circle paths A-B (**b**), C-D (**c**), E-F (**d**) and G-H (**e**). Nearby shoreline succession locations are shown above the cross-sections.

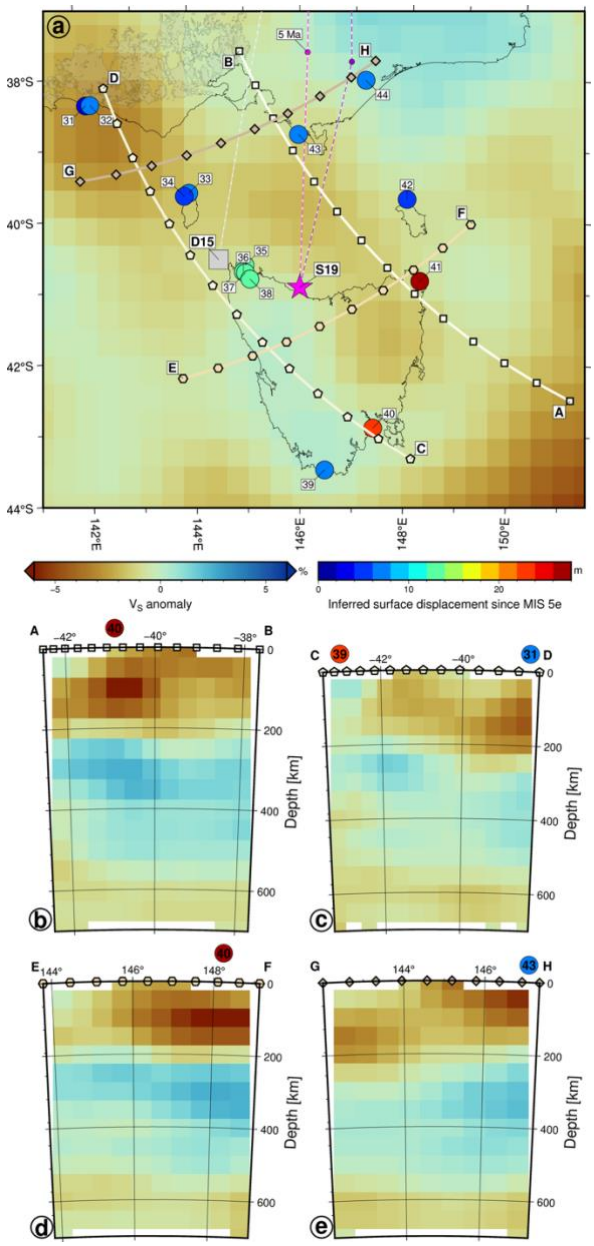

Figure 16. Inferred surface displacement of Last Interglacial shoreline successions and seismic tomography. a, Seismic tomography model REVEAL (Thrastarson et al., 2024) at 200 km depth, and Last Interglacial shoreline successions at 14 locations (Table 1) shown as disks coloured by inferred surface displacement assuming a 4 m APSL sea level during MIS 5e. Quaternary volcanic formations (GA, 2012) are shown as transparent grey polygons with a black outline. The reconstructed Cosgrove hotspot track is shown as a cyan dashed line and a grey square labelled 'D15' for the inferred present-day location based on the original publication (Davies et al., 2015), and as magenta and purple dashed lines for two alternative reconstructions by Seton et al. (2019), ending at the inferred present-day location shown as a

magenta star labelled ‘S19’. Cross-sections along small circles A-B, C-D, E-F, and G-H are shown with symbols matching panels b-e. Cross-sections of seismic topography model REVEAL down to 700 km depth along small-circle paths A-B (**b**), C-D (**c**), E-F (**d**) and G-H (**e**). Nearby shoreline succession locations are shown above the cross-sections.

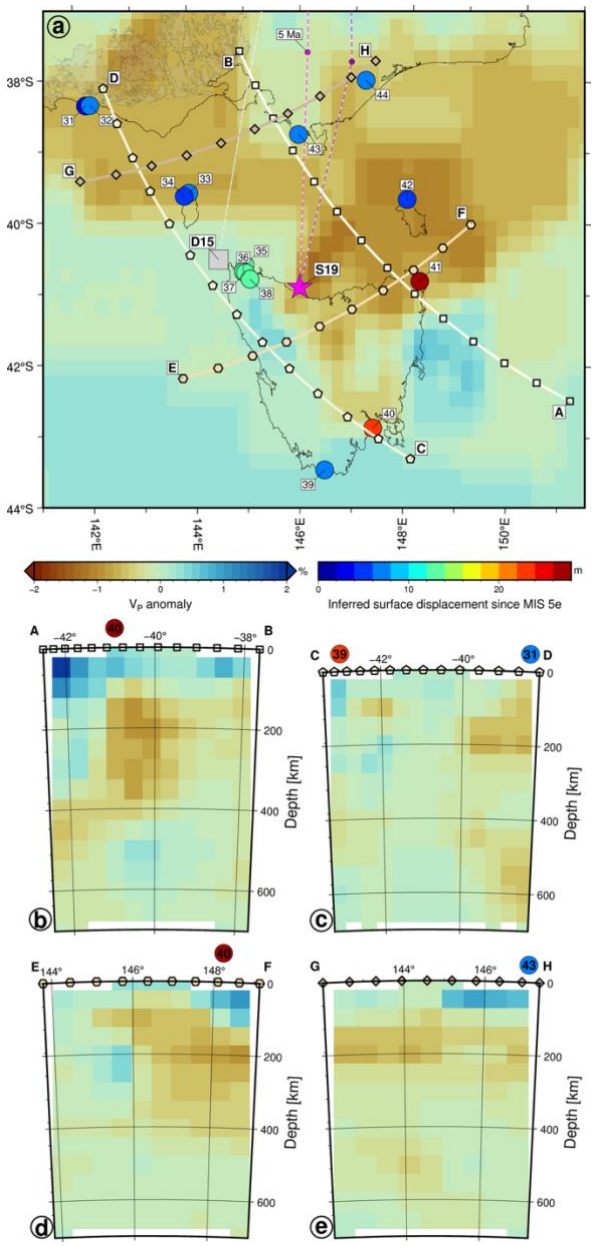

Figure 17. Last Interglacial shoreline elevation and seismic tomography. a, Seismic tomography model UU-P07 (Amaru, 2007) at 185 km depth, and Last Interglacial shoreline elevation at 14 locations (Table 1) shown as disks coloured by elevation. Disk outlines are black for paleoshorelines with present-day elevation greater than nine meters, and grey for other locations. Quaternary volcanic formations (GA, 2012) are shown as transparent grey polygons with a black outline. The reconstructed Cosgrove hotspot track is shown as a cyan dashed line and a grey square labelled ‘D15’ for the inferred present-day location based on the original publication (Davies et al., 2015), and as magenta and purple dashed lines for two alternative reconstructions by Seton et al. (2019), ending at the inferred present-day location

shown as a magenta star labelled 'S19'. Cross-sections along small circles A-B, C-D, E-F, and G-H are shown with symbols matching panels **b-e.** Cross-sections of seismic topography model UU-P07 down to 700 km depth along small-circle paths A-B (**b**), C-D (**c**), E-F (**d**) and G-H (**e**). Nearby paleoshorelines locations are projected above the cross-sections and labelled with numbers.

Positive seismic velocity anomalies suggest that a hot mantle could be the driver of uplift since MIS 5e in Tasmania, because hotter mantle is seismically slower and because sources of buoyancy closer to the surface are expected to result in greater dynamic uplift (Hager and Clayton, 1989). In S-wave tomographic model REVEAL (Thrastarson et al., 2024), the V_S anomaly is less pronounced under Tasmania and restricted to the uppermost 200 km (Fig. 16). While there is a pronounced anomaly at ~100 km beneath Mary Ann Bay (location 40) in that model, there is no V_S anomaly under Stumpys Bay (location 40; Figure 16b-e). Shallow anomalies beneath Warrnambool and Sale (locations 32 and 44, inferred uplift ~6.5 m) in S-wave tomographic model REVEAL are probably in the lithosphere (Fig. 13). In P-wave tomographic model UUP-7 (Amaru, 2007), there is a clear V_P anomaly beneath northeastern Tasmania at 185 km depth (Fig. 17a). There is a V_P anomaly between ~100–375 km depths close to Sale (location 44; Fig. 17b, d), no anomaly beneath Mary Ann Bay (location 40), and a possible shallow anomaly beneath Warrnambool (location 32). Overall, the three considered seismic tomographic models suggest that hot mantle between ~100–400 km depth could explain inferred uplift since MIS 5e in Tasmania, particularly in the northeast part of Tasmania.

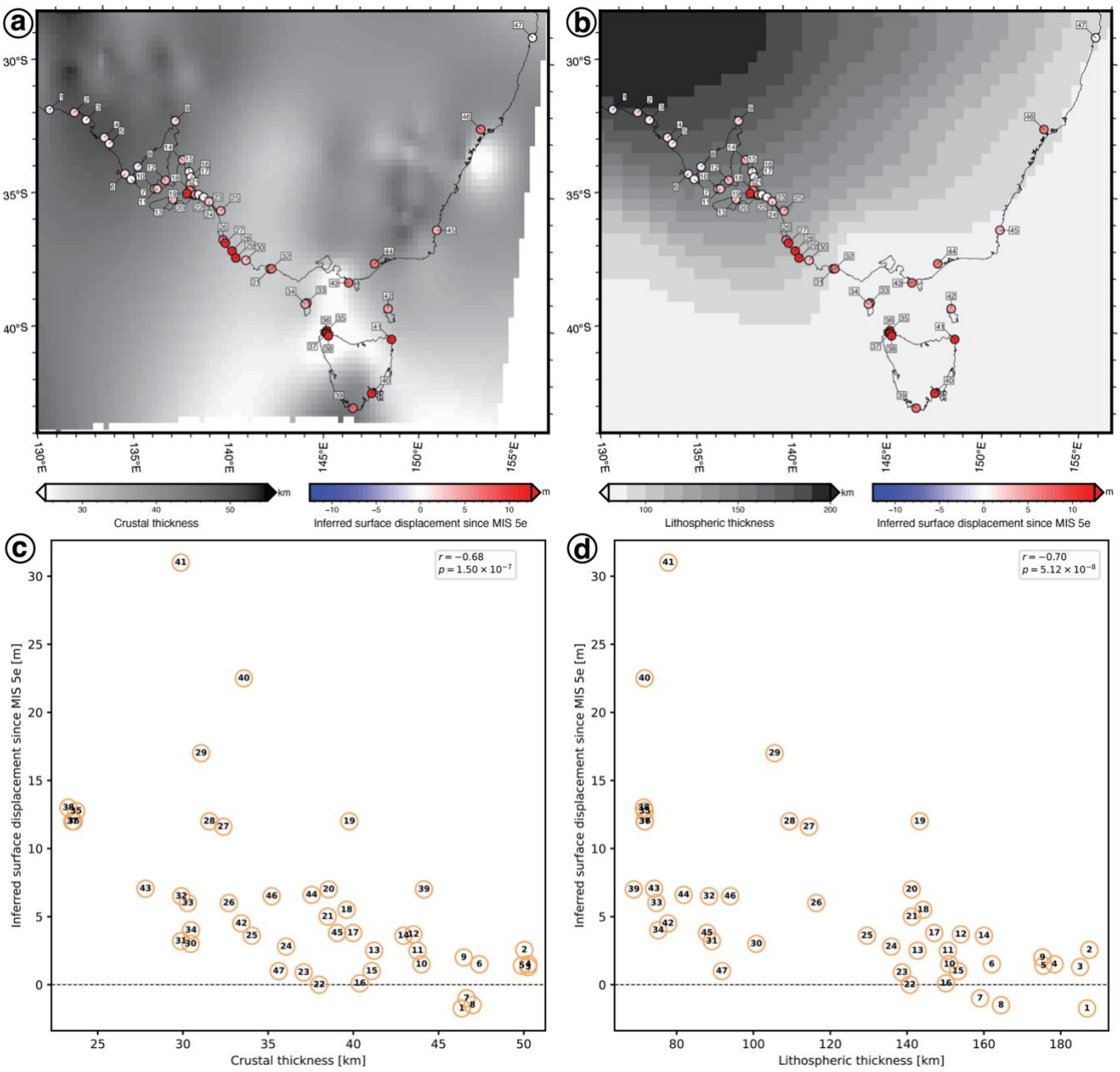

Figure 18. Inferred surface displacement of Last Interglacial shoreline successions, crustal thickness and lithospheric thickness. a, Crustal thickness (Stephenson et al., 2024), **b**, lithospheric thickness (Hoggard et al., 2020) and inferred surface displacement of Last Interglacial coastal successions at 47 locations (Table 1) shown as disks coloured by inferred surface displacement assuming a sea level 4 m higher during the Last Interglacial. **c-d**, Inferred surface displacement of Last Interglacial shoreline successions as a function of crustal (**c**) and lithosphere (**d**) thickness. *r* is the Spearman correlation coefficient, and *p* is the *p*-value for a Spearman ranking test with null hypothesis that two samples have no ordinal correlation.

3.3.2. Crustal thickness

A statistically significant Spearman anticorrelation (r = -0.68) indicates that inferred surface displacement since MIS 5e generally decrease as crustal thickness increases (Fig. 18c).

The thickness of the continental crust is less than ~34 km at the Tasmanian locations of interest (Fig. 18a, c). In map view, the model of Stephenson et al. (2024) predicts the thinnest crust beneath northwestern Tasmania, which could explain why inferred uplift since MIS 5e is large there even though the area is not directly above slow seismic anomalies (Fig. 15): dynamic uplift would be more significant because the convecting mantle would be closer to the surface (Hager and Clayton, 1989). Significant uplift since MIS 5e times between the McCourt Cutting and Nene Valley (locations 27-29, ~12-17 m) and at Normanville (location 19, 12 m) is not well explained by crustal thickness (~32-42 km thick, Fig. 18c).

3.3.3. Lithospheric thickness

In southeastern Australia, lithospheric thickness increases from the southeast to the northwest (Fig. 18b). Thin (< 80 km thick) lithosphere occurs in Tasmania, where the largest uplift since MIS 5e is inferred, and thick lithosphere occurs in the Gawler Craton, with lithosphere thicker than 160 km at the Fowlers Bay, Port Lincoln, and Tumby Bay (locations 1, 7, and 8) where 1 m to 1.75 m of subsidence was inferred since MIS 5e (Figs 8b and 13d). There is a statistically significant Spearman ranking anticorrelation (r = -0.70) between lithospheric thickness and inferred surface displacement since MIS 5e (Fig. 18d). This general trend suggests that lithospheric thickness could influence surface displacement since MIS 5e in the region because mantle convection at shallower depths results in greater dynamic topography (Hager and Clayton, 1989). Significant uplift since MIS 5e times between McCourt Cutting and Nene Valley (locations 27-29, ~12-17 m) and at Normanville (location 19, 12 m) is not well explained by lithospheric thickness (~110-145 km, Fig. 18b, d).

912 3.3.4. Residual topography

913 Residual topography is the difference between observed topography and the topography
914 expected from an isostatic model. Residual topography indicates the effect of mantle
915 convection on topography, a limit being the uncertainty in the isostatic model. In the global
916 continental residual topography model of Stephenson et al. (2024), residual topography
917 (Fig. 19a) closely depends on crustal thickness (Fig. 18a), with more positive residual
918 topography where the crust is thinner (Figs 18a and 19a). There is a statistically significant
919 Spearman ranking correlation ($r = 0.62$) indicating reasonable agreement between this residual
920 topography model and inferred surface displacement since MIS 5e (Fig. 19c). Large (~800 m)
921 residual topography could explain the inferred large uplift of MIS 5e shorelines (12–13 m) in
922 northwest Tasmania, and negative residual topography (between approximately -650 m and
923 approximately -20 m) is predicted for the three locations in the Gawler Craton for which some
924 subsidence was inferred (Fig. 19c). Significant uplift of MIS 5e shoreline successions between
925 McCourt Cutting and Nene Valley (locations 27 and 29, ~12-17 m) also correspond with
926 positive residual topography (~180–210 m). However, residual topography is only predicted to
927 be ~200 m in northeast Tasmania, where the inferred uplift since MIS 5e times elevation is
928 largest (31 m), and residual topography is predicted to be negative (approximately -500 m) in
929 southeast Tasmania, where the inferred uplift since MIS 5e times is large (22.5 m) and at
930 Normanville (location 19, approximately -180 m), where the inferred uplift is 12 m (Fig. 19a,c).

931 Stephenson et al. (2024) found that positive residual topography tends to be associated with
932 lithosphere thinner than ~100 km. While positive residual topography tends to be associated
933 with thin lithosphere in southeastern Australia (Figs 18b and 19a), there are exceptions in
934 southeastern Tasmania and to some extent in the area between Lake Hawdon South and Nene
935 Valley (locations 26-29), which is above a steep gradient in lithospheric thickness (Fig. 18b).

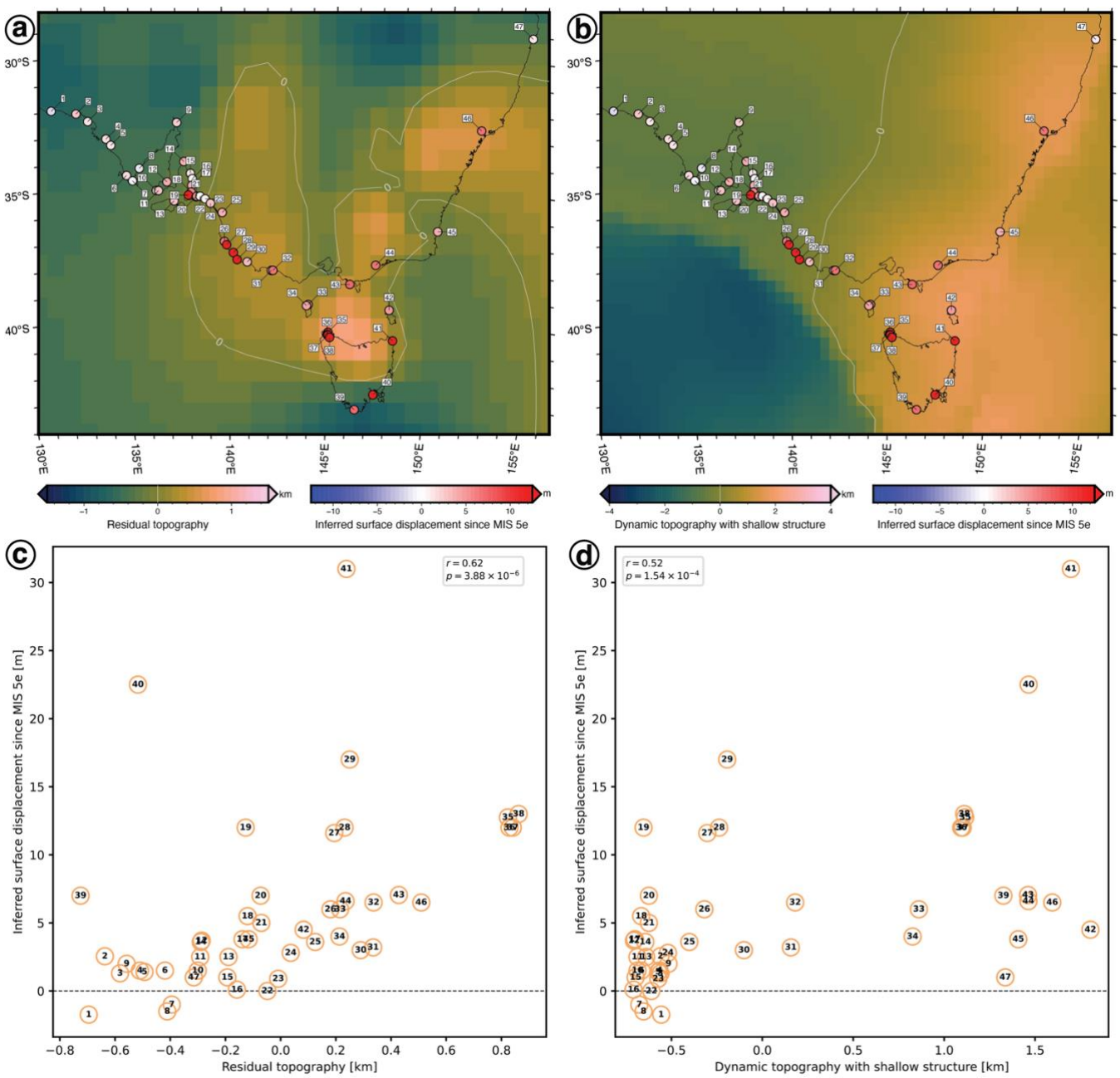

Figure 19. Inferred surface displacement of Last Interglacial shoreline successions, residual topography, and dynamic topography. a, Residual topography (Stephenson et al., 2024), **b**, dynamic topography (Davies et al., 2019), and Last Interglacial coastal successions at 47 locations (Table 1) shown as disks coloured by inferred surface displacement assuming a sea level 4 m higher during the Last Interglacial. **c-d**, Inferred surface displacement of Last Interglacial shoreline successions as a function of residual topography (**c**) and dynamic topography (**d**). *r* is the Spearman correlation coefficient, and *p* is the *p*-value for a Spearman ranking test with null hypothesis that two samples have no ordinal correlation.

3.3.5. Dynamic topography

Dynamic topography, which is the surface deflection predicted by a mantle flow model, depends on the distribution of sources of buoyancy and on the viscosity structure of the mantle

(Flament et al., 2013; Hager and Clayton, 1989). A dynamic topography model that considers the structure of the lithosphere (Davies et al., 2019) presents some agreement with the inferred surface displacement of MIS 5e shoreline successions, with a statistically significant Spearman ranking correlation (r = 0.52, Fig. 19d). The model suggests that positive dynamic topography (> 1 km) could be contributing to the inferred uplift in Tasmania, and negative dynamic topography (< -0.5 km) is predicted for the three locations in the Gawler Craton for which subsidence was inferred (Fig. 19d). However, the predicted large positive dynamic topography (> 1.3 km) is at odds with limited inferred uplift in Bass Strait and on the East coast of Australia, and negative dynamic topography (<-0.5 km) is at odds with the inferred uplift between McCourt Cutting and Nene Valley (locations 27-29, ~12-17 m) and at location Normanville (location 19, 12 m, Fig. 19b,d).

4. Discussion: global, regional and local drivers of MIS 5e paleoshoreline elevations

4.1. MIS 5e sea level in southeastern Australia and globally

4.1.1. Inferred amplitude of MIS 5e peak sea level: globally and in southeastern Australia

There has been much discussion about the height of the sea surface during the MIS 5e highstand. In a compilation of paleosea level observations from Indo-Pacific coralline successions remote from plate boundaries, Veeh (1966) documented relative sea levels of 2–9 m APSL. From these values a *de facto* value of 6 m APSL emerged in the literature for the MIS 5e highstand, which was consolidated by observations by Neumann and Moore (1975) in the northern Bahamas and by Ku et al. (1974) in Hawaii. Studies of neotectonism at plate boundaries consolidated the 6 m APSL value which was used commonly in calculations of uplift rates (Murray-Wallace and Woodroffe, 2014).

Based on statistical modelling, Kopp et al. (2009) concluded that there is a 95% probability that global sea level reached at least 6.6 m APSL during MIS 5e, as distinct from local sea levels. The highstand is an indication of global mean sea level, which is proposed to have ranged between 6 and 9 m during MIS 5e (Dutton et al., 2015; Lambeck et al., 2012). Even in tectonically highly stable areas, sea level observations are affected by evolving dynamic topography and glacial isostatic adjustments (Dutton et al., 2015), reducing the overall resolution in quantifying ice-equivalent sea level at a global scale. Whilst observations of peak sea level may be useful to infer the peak in global mean sea level, the range in sea level proxies for a given area and period may contain information about climatic or tectonic influences on sea level. The MIS 5e sea level range of 4 ± 1 m adopted in this study (Murray-Wallace, 2018; Murray-Wallace et al., 2016; Pan et al., 2018) is slightly below the MIS 5e eustatic sea level peak (> 6 m) proposed by Dutton et al. (2015). The southern Australian observations are more representative of an ice-equivalent sea level with limited postglacial adjustment in this far-field region (Conrad, 2013). The dynamic topography history of southern Australia could also explain why MIS 5e sea level is inferred to have peaked at around 4 m in southeast Australia as opposed to 6 m. Keeping in mind that models are uncertain, at present-day, continental residual topography could be negative west of Bonney Reserve (location 24, Fig. 19a), oceanic residual topography could be negative west of Tasmania (Hoggard et al., 2017), and continental and dynamic topography could be negative west of Nelson (location 30, Fig. 19b). This negative residual and dynamic topography could explain why the inferred surface displacement in the Gawler Craton region is systematically less than in Western Australia (Murray-Wallace, 2002; O'Leary et al., 2013), where both oceanic and continental residual topography are presently positive (Hoggard et al., 2017; Stephenson et al., 2024) and neotectonic uplift is evident in the Cape Range region (Whitney and Hengesh, 2015).

999 4.1.2. Two sea level highstands during the Last Interglacial (MIS 5e)?

1000 The notion of a bipartite sea level highstand during the Last Interglacial (MIS 5e) was first
1001 documented from rapidly uplifting coastlines such as the Huon Peninsula in Papua New Guinea
1002 and eastern Indonesia, where well-dated coral reef successions are physically separated
1003 (Chappell and Thom, 1977; Chappell and Veeh, 1978). On Atauro Island, two distinct reef
1004 crests were noted of Last Interglacial age (Chappell and Veeh, 1978). On the Huon Peninsula,
1005 an early phase of reef development (Reef VIIa; 138±5 ka) was distinguished from a late phase
1006 (Reef VIIb; 118±2 ka), corresponding with uplift-corrected high sea level culminations of 5±5
1007 m and 6.5±4 m APSL respectively (Aharon and Chappell, 1986). A compound sea-level peak,
1008 however, is not evident in higher resolution oxygen isotope records from deep sea cores
1009 (Lisiecki and Raymo, 2005; Shackleton, 1987) or the EPICA Dome C ice-core record from
1010 Antarctica which reveals a single peak for MIS 5e (Masson-Delmotte et al., 2010).

1011 A compound sea level highstand is also not evident in Last Interglacial sedimentary
1012 successions in southeastern Australia, where exposures of facies architecture are sufficiently
1013 clear for detailed assessment. Two exposures of the Glanville and Upper Bridgewater
1014 Formations provide insights about the late-stage relative sea level history during MIS 5e in
1015 southeastern Australia. The sites show that sea level rose during MIS 5e, in the absence of two
1016 sea level highstands (Murray-Wallace et al., 2016; Pan et al., 2018).

1017 In a 3-km-long coastal cliff at Point Turton, Hardwicke Bay, southern Yorke Peninsula
1018 (location 12), the section reveals a single, upward deepening succession of bioclastic
1019 sediments, passing upwards from a basal unit of intertidal sand flat facies with abundant
1020 *Batillaria* (*Zeacumantus*) *diemenensis*, into richly fossiliferous shelly sands (coquina) of
1021 shallow subtidal origin, dominated by the bivalve mollusc *Katelysia* spp., and *Amesodesma*
1022 *angusta* (Pan et al., 2018). A bipartite sea level highstand is not evident from this sedimentary
1023 succession. At the time of deposition of the Glanville Formation at this locality, a seaway

(Peesey Swamp) existed across southern Yorke Peninsula linking southern Spencer Gulf with Gulf St Vincent (Pan et al., 2021; Fig. 20).

Figure 20. View looking southwest across Peesey Swamp, a landscape depression across southern Yorke Peninsula, southern Australia. The graded hillslope in the horizon extends up to 30 m APSL. Peesey Swamp is approximately 30 km long and represented a seaway during the Last Interglacial (MIS 5e) connecting southern Spencer Gulf and Gulf St Vincent. Detached calcrete blocks of the Last Interglacial Glanville Formation, containing fossil shells can be seen in the foreground and relate to deposition at the margin of the former seaway.

In the McCourt Cutting (location 27), a 1 km long drainage channel across the Last Interglacial Woakwine Range (Fig. 5d), near Robe in southern South Australia, a basal transgressive facies rises progressively landward, resting unconformably on an erosion surface formed on an older calcarenite of MIS 7 age (Murray-Wallace et al., 1999). The laterally persistent transgressive unit, comprising bioclastic sand and stringers of flint pebbles, extends up to 11.6 m APSL representing a relative sea-level rise, uncorrected for tectonic uplift, from 6.4 m to 11.6 m APSL. At the culmination of post-MIS 6 sea-level rise, an accumulation of indurated calcarenite clasts up to 40 cm (long-axis) were deposited on the seaward side of a

relict sea stack in the core of the Woakwine Range (Murray-Wallace et al., 1999). Separated by an irregular scour surface, the transgressive unit is overlain by a progradational succession of subtidal and overlying intertidal sediments which formed during the sea level highstand of MIS 5e. The contact between subtidal and intertidal facies dips in a seaward direction, falling steadily from 11.5 m to 6.2 m APSL uncorrected for neotectonic uplift, over a horizontal distance of 200 m within the McCourt Cutting, indicating a relative sea level fall of 5.3 m following the culmination of MIS 5e sea-level rise.

The Woakwine Range back-barrier estuarine-lagoonal facies with articulated intertidal cockles (*Katelysia rhytiphora* and *K. scalarina*) are overlain by landward advancing dune facies (Fig. 5e) and indicate a palaeosea-level of 9.2 m APSL, uncorrected for neotectonic uplift (Murray-Wallace et al., 1999). The back-barrier facies provide a more reliable paleosea-level estimate in view of the lower energy conditions at the time of sedimentation, in contrast to the higher wave energy that would have prevailed on the open ocean coastline. Assuming an ice-equivalent sea level of 4±1 m APSL during the Last Interglacial based on data from Eyre and Yorke peninsulas (Murray-Wallace et al., 2016; Pan et al., 2018) and noting that the landward limit of modern shelly gravel beaches occurs up to 2 m APSL, implies 5.6 m of uplift of the Woakwine Range at the site of McCourt Cutting since the Last Interglacial. A bipartite sea level highstand is not evident from this sedimentary succession, which tracks the culmination of the post-MIS 6 sea-level rise and the history of the MIS 5e highstand (Murray-Wallace et al., 1999).

The observations from the Glanville Formation about relative sea-level trends during the Last Interglacial are corroborated by a sedimentary succession at the North East River on northern Flinders Island, Bass Strait. Here, a Last Interglacial shoaling upwards estuarine succession reveals a transition from a basal accumulation of subtidal oyster bioherms, passing upwards through depauperate sands, culminating in three distinct shell beds (coquina –

1067 packstones) interbedded with bioclastic sand and minor shell fragments (Murray-Wallace and
1068 Goede, 1995; Fig. 5g, Fig. 7a,b). The mollusc packstones comprise mixed assemblages of
1069 articulated and disarticulated *Katelysia rhytiphora*, *Fulvia tenuicostata* and *Brachidontes* sp.,
1070 representing shallow subtidal to intertidal facies. The succession represents a relatively quiet
1071 water depositional environment within an estuary with good tidal exchange, and continued
1072 sediment aggradation during MIS 5e. The interbedded sand and coquina units represent lateral
1073 facies changes associated with sandflat development and sediment aggradation with the
1074 progressive loss of accommodation space within the North East River paleoestuary. A bipartite
1075 sea level high stand is not evident from the succession.

1076 The beach ridge plain on Robbins Island, northwestern Tasmania also does not indicate a
1077 bipartite sea level highstand during MIS 5e. The relative sea level record during MIS 5e is
1078 represented by three discrete phases: a sea level fall from 7 m to 6 m APSL between 130–
1079 126 ka, a stillstand at 5.75 ± 0.5 m APSL between 126–121 ka, and a subsequent fall in sea
1080 level between 119–114 ka (Goodwin et al., 2023). The overall pattern of sea level behaviour
1081 for the Robbins Island beach ridge succession is a progressive fall in sea level (forced
1082 regression) in accord with hydro-isostasy as noted from Last Interglacial and Holocene relative
1083 sea level records (Belperio et al., 2002; Lambeck et al., 2012; Nakada and Lambeck, 1989;
1084 Stirling et al., 1995). In summary, a bipartite sea level highstand for MIS 5e is not evident from
1085 four geographically widely separated sites in southeastern Australia at which a continuous
1086 record of MIS 5e sea-level change is preserved.

1087

1088 **4.2. A waning mantle plume at the end of the longest continental hotspot track**

1089 Our main finding is that the inferred uplift since MIS 5e by 7 m to 31 m on the main island
1090 of Tasmania (Figs 8–9) could be explained by seismically slow (and therefore hot) mantle
1091 beneath Tasmania (Figs 15–17). This model fits to first order with reconstructions of the

Cosgrove track, from which the hotspot is inferred to be presently located under northern Tasmania (Figs 8, 14–17). The Cosgrove hotspot track (Davies et al., 2019), and the offshore Tasmantid and Lord Howe hotspot tracks (Seton et al., 2019) present decreasing ages of volcanic formations from north to south, however, their geophysical and geochemical signatures suggest that they may not be linked to a deep mantle plume (Jackson et al., 2021). A recent model proposes that eastern Australian mantle plumes could be restricted to the upper mantle, with fluctuations in magmatic activity from 60 Ma controlled by slab flux along the southwest Pacific (Mather et al., 2020). The absence of Quaternary volcanism in Tasmania (Fig. 8) suggests a waning Cosgrove mantle plume in which temperature anomalies are no longer large enough to trigger melting and volcanic eruptions. However, the Cosgrove mantle plume may still be buoyant enough to result in positive residual and dynamic topography (Fig. 19) above thin continental crust and lithospheric mantle (Fig. 18), and to drive the inferred uplift of MIS 5e shorelines by up to 31 m (Fig. 8b). A continental-scale compilation of temperature at 5 km depth (GA, 2021) reveals elevated temperatures in northeastern Tasmania, suggesting that the waning Cosgrove plume may still be hot enough to result in large geothermal gradients, which is reminiscent of a waning plume model previously proposed for eastern Europe (Ismail-Zadeh et al., 2024).

The inferred uplift on King Island and Flinders Island (locations 33, 34 and 42) in Bass Strait is relatively low (4.5 m to 6 m), even though they tend to be above seismically slow mantle (Figs 15-17). This discrepancy might be explained by continuing subsidence in Bass Basin (Middleton, 1982). Alternatively, these elevations may suggest that the waning Cosgrove mantle plume is located farther south under the main island of Tasmania.

Tomographic models suggest that the waning Cosgrove plume could be further east than previously inferred from hotspot tracks (Figs 8, 14-17; Davies et al., 2019; Seton et al., 2019), keeping in mind that the location of a plume is better characterised by a region than by discrete

points that are most convenient to represent hotspot tracks. A related question is the relationship between the Newer Volcanic Province and the Cosgrove plume. While early volcanic activity (between 7.9 Ma and ~4 Ma) in the Newer Volcanic Province (Heath et al., 2020) would temporally fit with the inferred latitude of the Cosgrove plume at these times (Fig. 8a), the eastern edge of the Newer Volcanic Province is ~200 km west from the western-most reconstructed Cosgrove hotspot track (Fig. 8a; Seton et al., 2019), which would require asthenospheric flow over 200 km without surface expression. Instead, volcanic activity in the Newer Volcanic Province between 7.9 Ma and 0.8 Ma (Heath et al., 2020) has been linked to edge-driven convection at the trailing edge of a fast moving plate (Farrington et al., 2010), with a heat source restricted to the upper mantle (Davies and Rawlinson, 2014). Volcanic activity from ~700 ka at the Mount Burr Volcanic Complex and in the past 5,000 years at Mount Gambier and Mount Schank (Barbetti and Sheard, 1981; Robertson et al., 1996) is within 70 km of the Newer Volcanic Province (Fig. 12), and could be a continuation of edge-driven convection, favoured by crustal enrichment in CO_2 (Chivas et al., 1987).

4.3. Local drivers of MIS 5e shoreline elevations

The elevated MIS 5e shoreline at Normanville, Fleurieu Peninsula (location 19) can be explained by uplift of the Kangarilla Fault Block to the southeast of the Willunga Fault (Fig. 11). The Willunga Fault is a Cambrian rift fault reactivated as a thrust fault during the Delamerian Orogeny (c. 510–490 Ma; Foden et al., 2006), and again in compression from Eocene times (Preiss, 2019). Movement on the Willunga Fault is also evident from the deposition of the Ochre Cove Formation, a succession of proximal alluvial gravels at Sellicks Beach, which have been dated to Early-Middle Pleistocene age based on magnetostratigraphy (Pillans and Bourman, 2001). This suggests that the uplift of the Normanville location could

be driven by reactivation of the Willunga Fault under the current thrust-strike slip fault local stress regime (Rajabi et al., 2017).

The increase in MIS 5e shoreline elevations between Lake Hawdon South to Nene Valley (locations 26-29) could be linked to volcanic activity at Mount Schank and Mount Gambier (Murray-Wallace, 2018; Sprigg, 1952). It is noted that the decrease in inferred uplift since MIS 5e times between Nene Valley and Nelson (locations 29 and 30, 14 m over 40 km) is more rapid than the increase between Lake Hawdon South and Nene Valley (locations 26-29, 11 m over 100 km). Sprigg (1952) defined an axis separating opposing slopes, which he termed the Mt Gambier Upwarp (Fig. 12). The broadly linear axis trends northeast-southwest and truncates the mid-point of a dome on the upper surface of the Oligo-Miocene Gambier Limestone. According to Sprigg (1952), the Mt Gambier Upwarp is situated mid-way between the Pleistocene and Holocene volcanic centres, approximately 10 km west of Mount Gambier. The origin of this asymmetry could be elucidated by further mapping of geological structures including the upper surface of the Gambier limestone, and by the characterisation of further MIS 5e shoreline successions between Nene Valley and Nelson.

Conclusions

1. The present-day elevation and paleosea levels of 47 shoreline successions in southeastern Australia make it possible to infer surface displacement since their deposition during MIS 5e times. The paleosea levels suggest that sea level was 4 ± 1 m higher during the Last Interglacial than at present. This sea level is approximately two metres lower than the commonly assumed global MIS 5e sea level peak, which could be explained by a limited postglacial response in this region in the far-field of Pleistocene ice sheets. There is no evidence for two

MIS 5e sea-level peaks from the four distant sites at which a continuous record of MIS 5e sea-level change is preserved.

2. The inferred uplift since MIS 5e is largest in Tasmania, where it is likely caused by the waning Cosgrove mantle plume. Seismic tomographic models and the locations with largest inferred uplift of MIS 5e shoreline successions in Tasmania suggest that the Cosgrove hotspot could be farther east than previously proposed. Volcanic activity from ~700 ka at the Mount Burr volcanic complex and ~5 ka at Mount Gambier and Mount Schank caused tilting of the Coorong coastal plain by up to ~10 m to the southeast since MIS 5e times. This volcanic activity is favoured by crustal enrichment in CO_2, and it could be driven by mantle convection along a steep lithospheric thickness gradient at the trailing edge of a fast-moving plate

3. Fleurieu Peninsula is tectonically active, and the inferred surface displacements suggest reactivation of the Willunga Fault accommodating 6.5 m of upward displacement of the block to its southeast since MIS 5e times. In contrast, the Gawler craton is inferred to have been stable since MIS 5e times, with possible limited local subsidence.

Acknowledgments

NF and CVMW were supported by ARC DP200101591. NF was supported by ARC FT230100001. The underlying basis for this research commenced in the early 1990s when CVMW started field investigations on the Quaternary geological history of the Coorong Coastal Plain in southern South Australia, involving many field investigations. CVMW acknowledges research support from the Australian Research Council over many years that made this work possible.

Author contributions (CRediT author statement)

Both authors contributed equally to the work. **Nicolas Flament:** Conceptualization, Methodology, Validation, Formal Analysis, Investigation, Writing – Original Draft, Visualization, Funding Acquisition. **Colin V. Murray-Wallace:** Conceptualization, Methodology, Validation, Formal Analysis, Investigation, Writing – Original Draft, Visualization, Funding Acquisition.

References

Aharon, P. and Chappell, J., 1986. Oxygen isotopes, sea level changes and the temperature history of a coral reef environment in New Guinea over the last 105 years. Palaeogeography, palaeoclimatology, palaeoecology, 56(3-4): 337-379.

Amaru, M., 2007. Global travel time tomography with 3-D reference models.

Barbetti, M. and Sheard, M., 1981. Palaeomagnetic results from Mounts Gambier and Schank, South Australia. Journal of the Geological Society of Australia, 28(3-4): 385-394.

Belperio, A., 1985. Quaternary geology of the Sandy Point and Outer Harbor-St. Kilda areas, Gulf St. Vincent, Quarterly Geological Notes. The Geological Survey of South Australia, pp. 2-6.

Belperio, A., 1993. Land subsidence and sea level rise in the Port Adelaide estuary: implications for monitoring the greenhouse effect. Australian Journal of Earth Sciences, 40(4): 359-368.

Belperio, A., Harvey, N. and Bourman, R., 2002. Spatial and temporal variability in the Holocene sea-level record of the South Australian coastline. Sedimentary Geology, 150(1-2): 153-169.

Belperio, A., Murray-Wallace, C. and Cann, J., 1995. The last interglacial shoreline in southern Australia: morphostratigraphic variations in a temperate carbonate setting. Quaternary International, 26: 7-19.

Blake, D.H., Kilgour, B., 1998. Geological Regions of Australia, 1:5 000 000 scale. In: G. Australia (Editor).

Blakemore, A., Murray-Wallace, C. and Lachlan, T., 2014. First recorded evidence of subaqueously-deposited late Pleistocene interstadial (MIS 5c) coastal strata above present sea level in Australia. Marine Geology, 355: 377-383.

Blakemore, A., Murray-Wallace, C.V., Westaway, K.E. and Lachlan, T.J., 2015. Aminostratigraphy and sea-level history of the Pleistocene Bridgewater Formation, Mount Gambier region, southern Australia. Australian Journal of Earth Sciences, 62(2): 151-169.

Bordoni, P. and Valensise, G., 1999. Deformation of the 125 ka marine terrace in Italy: tectonic implications. Geological Society, London, Special Publications, 146(1): 71-110.

Bourman, R. and Lindsay, J., 1989. Timing, extent and character of late Cainozoic faulting on the eastern margin of the Mt Lofty Ranges, South Australia. Transactions of the Royal Society of South Australia, 113(1-2): 63-67.

Bourman, R., Prescott, J., Banerjee, D., Alley, N. and Buckman, S., 2010. Age and origin of alluvial sediments within and flanking the Mt Lofty Ranges, southern South Australia:

a Late Quaternary archive of climate and environmental change. Australian Journal of Earth Sciences, 57(2): 175-192.
Bourman, R.P., Belperio, A., Murray-Wallace, C. and Cann, J., 1999. A last interglacial embayment fill at Normanville South Australia, and its neotectonic implications. Transactions of the Royal Society of South Australia, 123: 1-15.
Bourman, R.P., Murray-Wallace, C., Belperio, A. and Harvey, N., 2000. Rapid coastal geomorphic change in the River Murray Estuary of Australia. Marine Geology, 170(1-2): 141-168.
Bourman, R.P., Murray-Wallace, C.V. and Harvey, N., 2016. Coastal Landscapes of South Australia. University of Adelaide Press.
Bowden, A. and Colhoun, E., 1984. Quaternary emergent shorelines of Tasmania. In: B. Thom (Editor), Coastal Geomorphology in Australia. Academic Press, Sydney, pp. 313–342.
Cann, J. and Gostin, V., 1985. Coastal sedimentary facies and foraminiferal biofacies of the St Kilda Formation at Port Gawler, South Australia. Transactions of the Royal Society of South Australia, 109(4): 121-142.
Chappell, J., 1974. Geology of coral terraces, Huon Peninsula, New Guinea: a study of Quaternary tectonic movements and sea-level changes. Geological Society of America Bulletin, 85(4): 553-570.
Chappell, J. and Thom, B.G., 1977. Sea levels and coasts. Sunda and Sahul: 275-291.
Chappell, J. and Veeh, H., 1978. Late Quaternary tectonic movements and sea-level changes at Timor and Atauro Island. Geological Society of America Bulletin, 89(3): 356-368.
Chivas, A.R., Barnes, I., Evans, W.C., Lupton, J.E. and Stone, J.O., 1987. Liquid carbon dioxide of magmatic origin and its role in volcanic eruptions. Nature, 326(6113): 587-589.
Coe, A.L., 2003. The sedimentary record of sea-level change. Cambridge University Press.
Colhoun, E., Turner, E. and Van de Geer, G., 1982a. Late Pleistocene marine molluscan faunas from four sites in Tasmania. Papers and Proceedings of the Royal Society of Tasmania, 116: 91-96.
Colhoun, E., Van de Geer, G. and Mook, W., 1982b. Stratigraphy, pollen analysis, and paleoclimatic interpretation of Pulbeena Swamp, northwestern Tasmania. Quaternary research, 18(1): 108-126.
Conrad, C.P., 2013. The solid Earth's influence on sea level. Bulletin, 125(7-8): 1027-1052.
Crocker, R.L. and Cotton, B.C., 1946. Some raised beaches of the lower south-east of South Australia and their significance. Transactions of the Royal Society of South Australia, 70: 64-82.
Daniel, R., 2002. Carbonate sediments of a cool water embayment, Streaky Bay, South Australia. , University of Adelaide.
Davies, D., Rawlinson, N., Iaffaldano, G. and Campbell, I.H., 2015. Lithospheric controls on magma composition along Earth's longest continental hotspot track. Nature, 525(7570): 511-514.
Davies, D.R. and Rawlinson, N., 2014. On the origin of recent intraplate volcanism in Australia. Geology, 42(12): 1031-1034.
Davies, D.R., Valentine, A., Kramer, S.C., Rawlinson, N., Hoggard, M., Eakin, C. and Wilson, C.R., 2019. Earth's multi-scale topographic response to global mantle flow. Nature Geoscience, 12(10): 845-850.
De Mooy, C., 1959. Notes on the geomorphic history of the area surrounding Lakes Alexandrina and Albert, South Australia. Transactions of the Royal Society of South Australia, 82: 99-118.

Dutton, A., Carlson, A.E., Long, A.J., Milne, G.A., Clark, P.U., DeConto, R., Horton, B.P., Rahmstorf, S. and Raymo, M.E., 2015. Sea-level rise due to polar ice-sheet mass loss during past warm periods. science, 349(6244): aaa4019.

Eggins, S.M., Grün, R., McCulloch, M.T., Pike, A.W., Chappell, J., Kinsley, L., Mortimer, G., Shelley, M., Murray-Wallace, C.V. and Spötl, C., 2005. In situ U-series dating by laser-ablation multi-collector ICPMS: new prospects for Quaternary geochronology. Quaternary Science Reviews, 24(23-24): 2523-2538.

England, P. and Molnar, P., 1990. Surface uplift, uplift of rocks, and exhumation of rocks. Geology, 18(12): 1173-1177.

Fanning, C.M., Reid, A. and Teale, G., 2007. A geochronological framework for the Gawler Craton, South Australia. Bulletin, 55. Geological Survey of South Australia, 258 pp.

Farrington, R., Stegman, D.R., Moresi, L.-N., Sandiford, M. and May, D.A., 2010. Interactions of 3D mantle flow and continental lithosphere near passive margins. Tectonophysics, 483(1-2): 20-28.

Firman, J., 1966. Stratigraphic units of Late Cainozoic age in the St Vincent Basin, South Australia. Quarterly Geological Notes, Geological Survey of South Australia, 17: 6-9.

Flament, N., Gurnis, M. and Müller, R.D., 2013. A review of observations and models of dynamic topography. Lithosphere, 5(2): 189-210.

Foden, J., Elburg, M.A., Dougherty-Page, J. and Burtt, A., 2006. The timing and duration of the Delamerian Orogeny: correlation with the Ross Orogen and implications for Gondwana assembly. The Journal of Geology, 114(2): 189-210.

GA, 2012. Surface Geology of Australia. Geoscience Australia.

GA, 2019. National Gravity Compilation 2019 ground elevation ellipsoid image (hillshade HSI). In: G. Australia (Editor).

GA, 2021. Australian (OZTemp) Well Temperature Data Collection. In: G. Australia (Editor).

GA, 2024. Geoscience Australia Earthquake Catalogue.

Gardner, T., Webb, J., Pezzia, C., Amborn, T., Tunnell, R., Flanagan, S., Merritts, D., Marshall, J., Fabel, D. and Cupper, M.L., 2009. Episodic intraplate deformation of stable continental margins: evidence from Late Neogene and Quaternary marine terraces, Cape Liptrap, Southeastern Australia. Quaternary Science Reviews, 28(1-2): 39-53.

Gill, E., 1988. Warrnambool-Port Fairy district. In: J.G. Douglas and J.A. Ferguson (Editors), Geology of Victoria. Geological Society of Australia pp. 374-379.

Gill, E.D. and Banks, M.R., 1956. Cainozoic history of Mowbray Swamp and other areas of north-western Tasmania. Records of the Queen Victoria Museum, 6. Museum committee, Launceston City Council, Launceston, 41 pp.

Goodwin, I.D., Mortlock, T.R., Ribo, M., Mitrovica, J.X., O'Leary, M. and Williams, R., 2023. Robbins Island: The index site for regional Last Interglacial sea level, wave climate and the subtropical ridge around Bass Strait, Australia. Quaternary Science Reviews, 305: 107996.

Greenway, T. and Phillipps, H., 1902. Notes on the geological features of southern Yorke Peninsula. Transactions of the Royal Society of South Australia, 26: 268-277.

Hager, B.H. and Clayton, R.W., 1989. Constraints on the structure of mantle convection using seismic observations, flow models, and the geoid. Mantle convection, 657.

Hails, J., Belperio, A., Gostin, V. and Sargent, G., 1984. The submarine Quaternary stratigraphy of northern Spencer Gulf, South Australia. Marine Geology, 61(2-4): 345-372.

Harte, M., 1998. Superfamily Veneroidea. In: P. Beesley, G. Ross and A. Wells (Editors), Mollusca: The Southern Synthesis. Fauna of Australia. CSIRO Publishing, Melbourne.

Heath, M., Phillips, D. and Matchan, E., 2020. Basalt lava flows of the intraplate Newer Volcanic Province in south-east Australia (Melbourne region): 40Ar/39Ar geochronology reveals~ 8 Ma of episodic activity. Journal of Volcanology and Geothermal Research, 389: 106730.

Hoggard, M.J., Czarnota, K., Richards, F.D., Huston, D.L., Jaques, A.L. and Ghelichkhan, S., 2020. Global distribution of sediment-hosted metals controlled by craton edge stability. Nature Geoscience, 13(7): 504-510.

Hoggard, M.J., Winterbourne, J., Czarnota, K. and White, N., 2017. Oceanic residual depth measurements, the plate cooling model, and global dynamic topography. Journal of Geophysical Research: Solid Earth, 122(3): 2328-2372.

Hossfeld, P.S., 1950. The Late Cainozoic history of the south-east of South Australia. Transactions of the Royal Society of South Australia, 73(2): 232-279.

Howchin, W., 1888. Remarks on a geological section at the new graving dock, Glanville, with special reference to a supposed old land surface now below sea level. 10: 31-35.

Ismail-Zadeh, A., Davaille, A., Besse, J. and Volozh, Y., 2024. East European sedimentary basins long heated by a fading mantle upwelling. Nature Communications, 15(1): 3915.

Jackson, M., Becker, T. and Steinberger, B., 2021. Spatial characteristics of recycled and primordial reservoirs in the deep mantle. Geochemistry, Geophysics, Geosystems, 22(3): e2020GC009525.

Jenkin, J.J., 1988. Western Port and Southern Gippsland. In: J.G. Douglas and J.A. Ferguson (Editors), Geology of Victoria. Geological Society of Australia pp. 392-402.

Jennings, J.N., 1959. The coastal geomorphology of King Island, Bass Strait, in relation to changes in the relative level of land and sea. Records of the Queen Victoria Museum, Launceston, 11. Museum Committee, Launceston City Council.

JPL, N., 2013. NASA Shuttle Radar Topography Mission Global 3 arc second. In: N.L.P.D.A.A. Center (Editor).

Kiernan, K. and Lauritzen, S.-E., 2001. Dated speleothem evidence for uplift rates and terrace ages on the Tasmanian south coast. Zeitschrift für Geomorphologie, 45(6): 159–176.

Kopp, R.E., Simons, F.J., Mitrovica, J.X., Maloof, A.C. and Oppenheimer, M., 2009. Probabilistic assessment of sea level during the last interglacial stage. Nature, 462(7275): 863-867.

Kopp, R.E., Simons, F.J., Mitrovica, J.X., Maloof, A.C. and Oppenheimer, M., 2013. A probabilistic assessment of sea level variations within the last interglacial stage. Geophysical Journal International, 193(2): 711-716.

Ku, T.-L., Kimmel, M.A., Easton, W.H. and O'Neil, T.J., 1974. Eustatic sea level 120,000 years ago on Oahu, Hawaii. Science, 183(4128): 959-962.

Lambeck, K. and Chappell, J., 2001. Sea level change through the last glacial cycle. Science, 292(5517): 679-686.

Lambeck, K., Purcell, A. and Dutton, A., 2012. The anatomy of interglacial sea levels: the relationship between sea levels and ice volumes during the Last Interglacial. Earth and Planetary Science Letters, 315: 4-11.

Lisiecki, L.E. and Raymo, M.E., 2005. A Pliocene-Pleistocene stack of 57 globally distributed benthic δ18O records. Paleoceanography, 20(1).

Ludbrook, N., 1976. The Glanville Formation at Port Adelaide, Quarterly Geological Notes. The Geological Survey of South Australia.

Ludbrook, N., 1984. Quaternary molluscs of South Australia, 9. Department of Mines and Energy, South Australia, 327 pp.

Macpherson, J. and Gabriel, C., 1962. Marine molluscs of Victoria. Melbourne University Press, Melbourne.

Marshall, J. and Thom, B., 1976. The sea level in the last interglacial. Nature, 263(5573): 120-121.
Masson-Delmotte, V., Stenni, B., Pol, K., Braconnot, P., Cattani, O., Falourd, S., Kageyama, M., Jouzel, J., Landais, A. and Minster, B., 2010. EPICA Dome C record of glacial and interglacial intensities. Quaternary Science Reviews, 29(1-2): 113-128.
Mather, B.R., Müller, R.D., Seton, M., Ruttor, S., Nebel, O. and Mortimer, N., 2020. Intraplate volcanism triggered by bursts in slab flux. Science Advances, 6(51): eabd0953.
Middleton, M., 1982. The subsidence and thermal history of the Bass basin, Southeastern Australia. Tectonophysics, 87(1-4): 383-397.
Montelli, R., Nolet, G., Dahlen, F. and Masters, G., 2006. A catalogue of deep mantle plumes: New results from finite-frequency tomography. Geochemistry, Geophysics, Geosystems, 7(11).
Murray-Wallace, C. and Belperio, A., 1991. The last interglacial shoreline in Australia—a review. Quaternary Science Reviews, 10(5): 441-461.
Murray-Wallace, C., Belperio, A., Cann, J., Huntley, D. and Prescott, J., 1996a. Late Quaternary uplift history, Mount Gambier region, South Australia. Zeitschrift für Geomorphologie. Supplement Band(106): 41-56.
Murray-Wallace, C., Beu, A., Kendrick, G., Brown, L., Belperio, A. and Sherwood, J., 2000. Palaeoclimatic implications of the occurrence of the arcoid bivalve Anadara trapezia (Deshayes) in the Quaternary of Australasia. Quaternary Science Reviews, 19(6): 559-590.
Murray-Wallace, C. and Bourman, R., 2002. Amino acid racemisation dating of a raised gravel beach deposit, Sellicks Beach, South Australia. Transactions of the Royal Society of South Australia, 126: 21-28.
Murray-Wallace, C., Goede, A. and Picker, K., 1990. Last Interglacial coastal sediments at Mary Ann Bay, Tasmania, and their neotectonic significance. Quaternary Australasia, 8: 26-32.
Murray-Wallace, C., Leary, S. and Kimber, R., 1996b. Amino acid racemisation dating of a last interglacial estuarine deposit at Largs, New South Wales, Proceedings-Linnean Society Of New South Wales. Linnean Society Of New South Wales, pp. 213-222.
Murray-Wallace, C.V., 2011. Comment on:" New 40 Ar/39 Ar ages for selected young (< 1 Ma) basalt flows of the Newer Volcanic Province, southeastern Australia" by E. Matchan & D. Phillips. Quaternary Geochronology, 6(6): 598-599.
Murray-Wallace, C.V., 2018. Quaternary history of the Coorong coastal plain, southern Australia. Springer.
Murray-Wallace, C.V., Belperio, A., Bourman, R., Cann, J. and Price, D., 1999. Facies architecture of a last interglacial barrier: a model for Quaternary barrier development from the Coorong to Mount Gambier Coastal Plain, southeastern Australia. Marine Geology, 158(1-4): 177-195.
Murray-Wallace, C.V., Belperio, A., Dosseto, A., Nicholas, W.A., Mitchell, C., Bourman, R.P., Eggins, S.M. and Grün, R., 2016. Last interglacial (MIS 5e) sea-level determined from a tectonically stable, far-field location, Eyre Peninsula, southern Australia. Australian Journal of Earth Sciences, 63(5): 611-630.
Murray-Wallace, C.V., Bourman, R.P., Prescott, J.R., Williams, F., Price, D.M. and Belperio, A.P., 2010. Aminostratigraphy and thermoluminescence dating of coastal aeolianites and the later Quaternary history of a failed delta: The River Murray mouth region, South Australia. Quaternary Geochronology, 5(1): 28-49.

Murray-Wallace, C.V. and Cann, J., 2007. Quaternary history of the Coorong Coastal Plain, South Australia. XVII INQUA Congress, Excursion Guide A6. School of Earth & Environmental Sciences, University of Wollongong.

Murray-Wallace, C.V., Cann, J.H., Yokoyama, Y., Nicholas, W.A., Lachlan, T.J., Pan, T.-Y., Dosseto, A., Belperio, A.P. and Gostin, V.A., 2021. Late Pleistocene interstadial sea-levels (MIS 5a) in Gulf St Vincent, southern Australia, constrained by amino acid racemization dating of the benthic foraminifer Elphidium macelliforme. Quaternary Science Reviews, 259: 106899.

Murray-Wallace, C.V. and Goede, A., 1991. Aminostratigraphy and electron spin resonance studies of late Quaternary sea level change and coastal neotectonics in Tasmania, Australia. Zeitschrift für Geomorphologie, 35(2): 129-149.

Murray-Wallace, C.V. and Woodroffe, C.D., 2014. Quaternary sea-level changes: a global perspective. Cambridge University Press.

Murray-Wallace, C. and Goede, A., 1995. Aminostratigraphy and electron spin resonance dating of Quaternary coastal neotectonism in Tasmania and the Bass Strait islands. Australian Journal of Earth Sciences, 42(1): 51-67.

Murray-Wallace, C.V., 2002. Pleistocene coastal stratigraphy, sea-level highstands and neotectonism of the southern Australian passive continental margin—a review. Journal of Quaternary Science: Published for the Quaternary Research Association, 17(5-6): 469-489.

Nakada, M. and Lambeck, K., 1989. Late Pleistocene and Holocene sea-level change in the Australian region and mantle rheology. Geophysical Journal International, 96(3): 497-517.

Neumann, A.C. and Moore, W.S., 1975. Sea level events and Pleistocene coral ages in the northern Bahamas. Quaternary Research, 5(2): 215-224.

Nichol, S. and Murray-Wallace, C.V., 1992. A partially preserved last interglacial estuarine fill: Narrawallee Inlet, New South Wales. Australian Journal of Earth Sciences, 39(4): 545-553.

Nicholas, W., Lachlan, T., Murray-Wallace, C.V. and Price, G.J., 2019. Amino acid racemisation and uranium-series dating of a last interglacial raised beach, Kingscote, Kangaroo Island, southern Australia. Transactions of the Royal Society of South Australia, 143(1): 1-26.

Nielsen, B.J., 1964. Studies of the genus Katelysia Romer 1857 (Mollusca, Lamellibranchiata). Memoirs of the National Museum of Victoria, Melbourne, 26: 219-257.

O'Leary, M.J., Hearty, P.J., Thompson, W.G., Raymo, M.E., Mitrovica, J.X. and Webster, J.M., 2013. Ice sheet collapse following a prolonged period of stable sea level during the last interglacial. Nature Geoscience, 6(9): 796-800.

Ollier, C., 1978. Tectonics and geomorphology of the Eastern Highlands. In: J. Davies and M. Williams (Editors), Landform evolution in Australia. Australian National University Press, Canberra, pp. 5-47.

Ollier, C., 1986. Early landform evolution. In: D. Jeans (Editor), The Natural Environment. Sydney University Press, Sydney, pp. 97-116.

Pan, T.-Y., Murray-Wallace, C., Bourman, R. and García, A., 2021. Peesey Swamp—a Last Interglacial (MIS 5e) marine corridor across southern Yorke Peninsula, southern Australia. Australian Journal of Earth Sciences, 68(7): 952-967.

Pan, T.-Y., Murray-Wallace, C.V., Dosseto, A. and Bourman, R.P., 2018. The last interglacial (MIS 5e) sea level highstand from a tectonically stable far-field setting, Yorke Peninsula, southern Australia. Marine Geology, 398: 126-136.

Pedoja, K., Husson, L., Johnson, M.E., Melnick, D., Witt, C., Pochat, S., Nexer, M., Delcaillau, B., Pinegina, T. and Poprawski, Y., 2014. Coastal staircase sequences reflecting sea-level oscillations and tectonic uplift during the Quaternary and Neogene. Earth-Science Reviews, 132: 13-38.

Pillans, B. and Bourman, R., 2001. Mid Pleistocene arid shift in southern Australia, dated by magnetostratigraphy. Soil Research, 39(1): 89-98.

Preiss, W., 2019. The tectonic history of Adelaide's scarp-forming faults. Australian Journal of Earth Sciences, 66(3): 305-365.

Preiss, W., Alexander, E., Cowley, W. and Schwarz, M., 2002. Towards defining South Australia's geological provinces and sedimentary basins. MESA Journal, 27: 39-52.

Prezant, R., 1998. Introduction – Subclass Heterodonta. In: P. Beesley, G. Ross and A. Wells (Editors), Mollusca: The Southern Synthesis, Fauna of Australia. CSIRO Publishing, Melbourne, pp. 301–307.

Quigley, M.C., Clark, D. and Sandiford, M., 2010. Tectonic geomorphology of Australia. In: P. Bishop and B. Pillans (Editors), Australian Landscapes. Geological Society, London, Special Publication, pp. 243-265.

Rajabi, M., Tingay, M., Heidbach, O., Hillis, R. and Reynolds, S., 2017. The present-day stress field of Australia. Earth-Science Reviews, 168: 165-189.

Raymond, O.L.e., Gallagher, R. (editor), Shaw, R., Yeates, A.N., Doutch, H.F., Palfreyman, W.D., Blake, D.H., Highet, L., 2023. Surface Geology of Australia 2012, 1:2.5 Million Scale - Faults. In: G. Australia (Editor).

Roberts, D., 1984. The genus Katelysia (Bivalvia: Veneridae) in southern Australia. Journal of the Malacological Society of Australia, 6(3-4): 191-204.

Robertson, G., Prescott, J. and Hutton, J., 1996. Thermoluminescence dating of volcanic activity at Mount Gambier, South Australia. Transactions of the Royal Society of South Australia, 120: 7-12.

Rovere, A., Ryan, D.D., Vacchi, M., Dutton, A., Simms, A.R. and Murray-Wallace, C.V., 2023. The World Atlas of Last Interglacial Shorelines (version 1.0). Earth Syst. Sci. Data, 15(1): 1-23.

Ryan, D.D., 2015. The Quaternary geomorphological evolution of the River Murray mouth and lakes region, southern Australia, University of Wollongong, 460 pp.

Sandiford, M., 2003. Neotectonics of southeastern Australia: linking the Quaternary faulting record with seismicity and in situ stress. In: R.R. Hillis and R.D. Müller (Editors), Evolution and Dynamics of the Australian Plate. Geological Society of Australia and Geological Society of America Special Publication, pp. 107-199.

Saputra, S.E.A., Fergusson, C.L., Dosseto, A., Dougherty, A. and Murray-Wallace, C.V., 2022. Late Quaternary neotectonics in the Bird's Head Peninsula (West Papua), Indonesia: implications for plate motions in northwestern New Guinea, western Pacific. Journal of Asian Earth Sciences, 236: 105336.

Schornick, J., 1973. Th-230/U-234 geochronology of marine shells from near Sale, E. Victoria, Australia. Proceedings of the Royal Society of Victoria, 86: 35-37.

Schwebel, D., 1984. Quaternary stratigraphy and sea-level variation in the southeast of South Australia. Coastal geomorphology in Australia: 291-311.

Seton, M., Williams, S., Mortimer, N., Meffre, S., Micklethwaite, S. and Zahirovic, S., 2019. Magma production along the Lord Howe seamount chain, northern Zealandia. Geological Magazine, 156(9): 1605-1617.

Shackleton, N., 1987. Oxygen isotopes, ice volume and sea level. Quaternary science reviews, 6(3-4): 183-190.

Shackleton, N.J., Chapman, M., Sánchez-Goñi, M.F., Pailler, D. and Lancelot, Y., 2002. The classic marine isotope substage 5e. Quaternary Research, 58(1): 14-16.

Shennan, I., 2015. Handbook of sea-level research: framing research questions. Handbook of sea-level research: 3-25.
Sherwood, J., Barbetti, M., Ditchburn, R., Kimber, R., McCabe, W., Murray-Wallace, C., Prescott, J. and Whitehead, N., 1994. A comparative study of Quaternary dating techniques applied to sedimentary deposits in southwest Victoria, Australia. Quaternary Science Reviews, 13(2): 95-110.
Slee, A.J., McIntosh, P.D., Price, D.M. and Groved, S., 2012. A reassessment of last interglacial deposits at Mary Ann Bay, Tasmania. Quaternary Australasia, 29(2): 4-11.
Spearman, C., 1904. The Proof and Measurement of Association between Two Things. The American Journal of Psychology, 15(1): 72-101.
Sprigg, R., 1959. Stranded sea beaches and associated sand accumulations of the upper southeast. Transactions of the Royal Society of South Australia, 82: 183-193.
Sprigg, R. and Boutakoff, N., 1953. Summary report on the petroleum possibilities of the Gambier Sunklands. Mining Review, Adelaide, 95: 41-62.
Sprigg, R.C., 1952. The Geology of the South-east Province of South Australia: With Special Reference to Quaternary Coast-line Migrations and Modern Beach Developments. Government Printer, South Africa.
Stephenson, S.N., Hoggard, M.J., Holdt, M.C. and White, N., 2024. Continental residual topography extracted from global analysis of crustal structure. Journal of Geophysical Research: Solid Earth, 129(4): e2023JB026735.
Stirling, C., Esat, T., McCulloch, M. and Lambeck, K., 1995. High-precision U-series dating of corals from Western Australia and implications for the timing and duration of the Last Interglacial. Earth and Planetary Science Letters, 135(1-4): 115-130.
Sutherland, F. and Kershaw, R., 1971. The Cainozoic geology of Flinders Island, Bass Strait, Papers and Proceedings of the Royal Society of Tasmania, pp. 151-178.
Tate, R., 1879a. The Anniversary address of the President, Transactions and Proceedings and Report of the Philosophical Society of Adelaide, South Australia, for 1878-1879, pp. XXXIX–IXXV.
Tate, R., 1879b. The natural history of the country around the head of the Great Australian Bight, Transactions and Proceedings and Report of the Philosophical Society of Adelaide, South Australia, for 1878-1879, 1–2.
Tate, R., 1882. The geology about Port Wakefield. Transactions and Proceedings and Report of the Royal Society of South Australia, 4: 45-46.
Thom, B. and Murray-Wallace, C., 1988. Geological note: last Interglacial (Stage 5e) estuarine sediments at Largs. New South Wales. Australian Journal of Earth Sciences, 35: 571-574.
Thrastarson, S., van Herwaarden, D.P., Noe, S., Josef Schiller, C. and Fichtner, A., 2024. REVEAL: A global full-waveform inversion model. Bulletin of the Seismological Society of America, 114(3): 1392-1406.
Twidale, C., 2007. Ancient Australian Landscapes. Rosenberg, Sydney, 144 pp.
Van de Geer, G., Colhoun, E. and Mook, W., 1986. Stratigraphy, pollen analysis and paleoclimatic interpretation of Mowrray and Broadmeadows Swamps, North Western Tasmania. Australian Geographer, 17(2): 121-133.
Veeh, H.H., 1966. Th230/U238 and U234/U238 ages of Pleistocene high sea level stand. Journal of Geophysical Research, 71(14): 3379-3386.
Whitney, B.B. and Hengesh, J.V., 2015. Geomorphological evidence for late Quaternary tectonic deformation of the Cape Region, coastal west central Australia. Geomorphology, 241: 160-174.
Woods, J.E., 1862. Geological observations in South Australia: principally in the district south-east of Adelaide. Longman, Green, Longman, Roberts, & Green.

1579 Young, R., Bryant, E. and Price, D., 1993. Last interglacial sea levels on the south coast of
1580 New South Wales. The Australian Geographer, 24(2): 72-75.

1581